OLD DOMINION UNIVERSITY RESEARCH FOUNDATION

DEPARTMENT OF PHYSICS
SCHOOL OF SCIENCES AND HEALTH PROFESSIONS
OLD DOMINION UNIVERSITY
NORFOLK, VIRGINIA

Technical Report PTR-80-3

TUNABLE DIODE LASER HETERODYNE RADIOMETER MEASUREMENT OF ATMOSPHERIC ABSORPTION OF SOLAR RADIATION

By

Charles N. Harward

and

Gary E. Copeland, Principal Investigator

Final Report
For the period October 15, 1977 - December 14, 1979

Prepared for the
National Aeronautics and Space Administration
Langley Research Center
Hampton, Virginia

Under
Research Grant NSG 1466
J.M. Hoell, Technical Monitor
Instrument Research Division

March 1980

DEPARTMENT OF PHYSICS
SCHOOL OF SCIENCES AND HEALTH PROFESSIONS
OLD DOMINION UNIVERSITY
NORFOLK, VIRGINIA

Technical Report PTR-80-3

TUNABLE DIODE LASER HETERODYNE RADIOMETER MEASUREMENT OF ATMOSPHERIC ABSORPTION OF SOLAR RADIATION

By

Charles N. Harward

and

Gary E. Copeland, Principal Investigator

Final Report
For the period October 15, 1977 - December 14, 1979

Prepared for the
National Aeronautics and Space Administration
Langley Research Center
Hampton, Virginia 23665

Under
Research Grant NSG 1466
J.M. Hoell, Technical Monitor
Instrument Research Division

Submitted by the
Old Dominion University Research Foundation
P.O. Box 6369
Norfolk, Virginia 23508

March 1980

TABLE OF CONTENTS

	Page
ABSTRACT	1
INTRODUCTION	1
EXPERIMENTAL DETAILS	2
MODE SCANS	3
IMPROVEMENTS IN CHARACTERIZATION PROCEDURES	5
SOLAR HETERODYNE MEASUREMENTS	8
CONCLUSIONS	14
ACKNOWLEDGMENTS	14
REFERENCES	15

LIST OF TABLES

Table		
1	Approximate wave number range of the lettered regions and atmospheric species which cause absorption	12

LIST OF FIGURES

Figure		
1	Optical schematic for heterodyne radiometer	16
2	TDL mode scans for currents from 0.25 to 1 35 A at 16 K	17
3	TDL mode scans for currents from 1.35 to 1.75 A at 16 K	18
4	1,000 K blackbody heterodyne signal and TDL-induced excess noise at 16 K for currents up to 1.9 A	19
5	TDL mode scans for currents from 0.30 to 1.30 A at 21 K	20
6	TDL mode scans for currents from 1.30 to 1.80 A at 21 K	21
7	1,000 K blackbody heterodyne signal and TDL-induced excess noise at 21 K for currents up to 1.90 A	22

LIST OF FIGURES (CONTINUED).

Figure		Page
8	1,000 K blackbody heterodyne signal and TDL-induced excess noise at 45 K for currents up to 1.90 A	23
9	1,000 K blackbody heterodyne signal and TDL-induced excess noise at 70 K for currents up to 1.90 A	24
10	Real time etalon scan of TDL modes (bottom trace) along with excess noise associated with TDL modes (top trace). Noise is increasing in downward direction	25
11	Single-mode 1,000 K blackbody heterodyne signal obtained with fixed spaced etalon as a mode isolator (top trace). Bottom trace shows the output of a 2.54-cm solid Ge etalon . .	26
12	Tracking control circuit for etalon	27
13	Single-mode 1,000 K blackbody heterodyne signal obtained with etalon peak locked to the TDL wavelength. Bottom trace shows the output of a 2.54-cm Ge etalon	28
14	Single-mode 1,000 K blackbody heterodyne signal obtained with etalon peak locked to the TDL wavelength. Bottom trace shows the output of a 2.54-cm Ge etalon. Temperature adjusted from figure 13 to increase the tuning range of TDL	29
15	Heterodyne atmospheric solar absorption spectrum along with directly detected HNO_3 spectrum	30
16	Simulated atmospheric spectrum generated from the line parameters and assumed profiles for HNO_3, CO_2, and H_2O	31
17	Simulated atmospheric spectrum generated from the line parameters and assumed profiles for HNO_3, CO_2, and H_2O. H_2O content is one-half that of figure 16	32
18	Heterodyne atmospheric solar absorption spectra along with etalon fringes obtained with the TDL temperature at 69.9 K . .	33
19	Fast Fourier transform atmospheric spectra from 1,050 to 1,075 cm^{-1} (Goldman et al., 1978)	34
20	Fast Fourier transform atmospheric spectra from 1,075 to 1,100 cm^{-1} (Goldman et al., 1978)	35
21	Heterodyne atmospheric solar absorption spectra along with etalon fringes obtained with the TDL temperature at 70.3 K. The current was scanned toward increasing currents	36

LIST OF FIGURES (CONTINUED).

Figure		Page
22	Heterodyne atmospheric solar absorption spectra along with etalon fringes obtained with the TDL temperature at 70.3 K. The current was scanned from high to low values	37
23	Heterodyne atmospheric solar absorption spectra along with etalon fringes obtained with the TDL temperature at 70.6 K. The current was scanned from low to high values	38
24	Heterodyne atmospheric solar absorption spectra along with etalon fringes obtained with the TDL temperature at 70.6 K. The current was scanned from high to low values	39
25	Heterodyne atmospheric solar absorption spectra along with etalon fringes obtained with the TDL temperature at 70.9 K. The current was scanned from low to high values	40
26	Heterodyne atmospheric solar absorption spectra along with etalon fringes obtained with the TDL temperature at 71.3 K. The current was scanned from low to high values	41
27	Heterodyne atmospheric solar absorption spectra along with etalon fringes obtained with the TDL temperature at 71.3 K. The current was scanned from high to low values	42
28	Heterodyne atmospheric solar absorption spectra along with etalon fringes obtained with TDL temperature at 72.0 K. The current was scanned from low to high values. Note expanded scale	43
29	Heterodyne atmospheric solar absorption spectra along with etalon fringes obtained with TDL temperature at 72.0 K. The current was scanned from high to low values	44
30	Heterodyne atmospheric solar absorption spectra along with etalon fringes obtained with TDL temperature at 72.5 K. The current was scanned from low to high values	45
31	Heterodyne atmospheric solar absorption spectra along with etalon fringes obtained with TDL temperature at 72.5 K. The current was scanned from high to low values	46
32	Heterodyne atmospheric solar absorption spectra along with etalon fringes obtained with TDL temperature at 73.0 K. The current was scanned from high to low values. Note new spectral region	47
33	Expanded heterodyne atmospheric solar absorption spectra along with etalon fringes obtained with TDL temperature at 71.3 K. The current was scanned in forward direction	48

LIST OF FIGURES (CONCLUDED).

Figure		Page
34	Expanded heterodyne atmospheric solar absorption spectra along with etalon fringes obtained with TDL temperature at 71.3 K. The current was scanned in reverse direction	49

TUNABLE DIODE LASER HETERODYNE RADIOMETER MEASUREMENT OF ATMOSPHERIC ABSORPTION OF SOLAR RADIATION

By

Charles N. Harward[1] and Gary E. Copeland[2]

ABSTRACT

A Tunable Infrared Heterodyne Radiometer (TIHR) which uses a diode laser as the local oscillator as well as methods for the evaluation of the excess noise characteristics of the Tunable Diode Laser (TDL) are described. Preliminary atmospheric absorption data taken with the TIHR are presented which show the capability of the TIHR for making the highest resolution atmospheric measurements to date.

INTRODUCTION

A Tunable Diode Laser (TDL) has been used as a local oscillator (LO) in a heterodyne radiometer coupled to a heliostat to measure the absorption of solar radiation by atmospheric constituents. The use of the TDL as an LO in a heterodyne system has been demonstrated only a limited number of times (Ku and Spears, 1977; Hackett, 1977; Mumma et al., 1975; and Harward, 1977). With the exception of Mumma et al. (1975), the heterodyne system has been used to detect radiation from a laboratory blackbody or the presence of gas in a cell through which laboratory blackbody radiation passes. The only other successful demonstration of the TDL as a LO was by Frerking and Muehlner (1977), who mounted a TDL along with the photomixer in a liquid nitrogen (LN_2) dewar. The use of LN_2 cooling limited the useful tuning range of the TDL and thus the number of atmospheric species that could be detected. In our present system the TDL is mounted in a commercial closed-cycle cooler.

---

[1] Research Assistant Professor, Department of Physics, Old Dominion University, Norfolk, Virginia 23508

[2] Associate Professor, Department of Physics, Old Dominion University, Norfolk, Virginia 23508

The wavelength tuning range of this TDL is now self-limited and extends from 8.9 to 11.2 cm^{-1}. Therefore the number of species which can be detected is greatly increased. For a few days near the end of the period covered by this grant, our present system was operated and the atmospheric species HNO_3, O_3, H_2O, and CO_2 were detected.

EXPERIMENTAL DETAILS

Figure 1 shows the optical schematic for the heterodyne radiometer. The TDL LO is mounted in a commercial closed-cycle cooler which has been modified to reduce frequency fluctuations that can be induced mechanically during the cooling cycle of the cooler. Radiation from the TDL is collected and collimated by the f/1 lens. For coarse wavelength identification or for isolation of a single TDL mode, the collimated radiation is refocused by an f/8 lens and passed through a monochromator. For single-mode operation or for use of the mode selection etalon, the monochromator is bypassed and the TDL radiation is combined with solar radiation via a 1:1 beam splitter. Solar radiation is directed to the beam splitter by a heliostat and is mechanically chopped and filtered using an eight-micron high-pass optical filter prior to the beam splitter. The combined TDL and solar radiation is focused onto a LN_2-cooled HgCdTe photomixer by an f/1 lens. The TDL radiation reflected by the beam splitter is mechanically chopped and divided by a second beam splitter One part is directed through a gas cell, and the other is directed through a 2.54-cm solid Ge etalon. Both portions of the chopped TDL radiation are focused onto LN_2-cooled HgCdTe detectors. These two legs make up the fine wavelength identification section of the Tunable Infrared Heterodyne Radiometer (TIHR).

The TIHR can be operated either as a scanning radiometer or at any fixed wavelength within the operating range of the TDL LO. In the former operational mode, the rf output from the photomixer is processed through a single IF filter. In the fixed wavelength operating mode the rf output is processed through an eight-channel IF filter bank. In either mode, the output from a second square law crystal detector following the IF filter(s) is synchronously detected. The fixed wavelength mode provides a multiplex advantage useful for quantitative

measurements of the vertical distribution of selected atmospheric species, and the scanning mode can be used in the selection of optimum regions for the fixed wavelength operational mode. The scanning mode spectra taken at different times of day can be used as input data to an iteration scheme to yield vertical profiles of selected atmospheric species.

MODE SCANS

For the successful operation of the TIHR, the spectral and excess noise characteristics of the TDL LO must be investigated. During the initial phases of our work, the spectral characteristics of the TDL as a function of current and temperature were investigated by using the monochromator to scan the TDL output. Figures 2 and 3 show the results of such mode scans. The operating temperature was 16 K, and the diode current was the independent variable. After each scan of the TDL modes, the current was increased by 0.1 A, the pen was offset from the previous scan by a small amount, and then a new mode scan was made. Figure 2 shows the laser modes for currents from 0.25 to 1.25 A, while figure 3 shows mode scans for currents from 1.25 to 1.75 A. The TDL lases in a single longitudinal mode at wavelengths of about 11.16 μ for a current between 0.25 to 0.45 A. This is shown in figure 2. Between 0.45 and 0.55 A it jumps to another single longitudinal mode at λ = 11.105 μ. This latter mode lases only over a small current range before jumping to another longitudinal mode with the addition of several small transverse modes. From currents of 1.45 to 1.65 A 2 longitudinal modes dominate the output of this TDL, but small transverse laser modes still appear. From these mode scans it can be concluded that this TDL can be used as an almost single-mode LO from threshold to a current of 0.95 A. Possibly it can be used as an LO from 1.45 to 1.65 A with some type of mode selection device.

Figure 4 indicates that this analysis is correct. The top trace in this figure shows the heterodyne signal obtained by beating the TDL against a 1,000 K blackbody. The intergrated noise in the output of IF amplifiers is shown in the lower trace. This is the excess noise induced by the TDL output. This noise has been limited to a 100-MHz bandwidth by a 100-MHz low-pass filter. The independent variable of

this figure is the current through the TDL. For certain currents the integrated noise increases very rapidly for small changes in TDL current, as seen in the lower trace of figure 4. Such increases occur at 0.5, 1.08, 1.23, 1.30 to 1.5 and around 1.7 A. These sudden increases in TDL-induced noise occur at currents where the TDL is in transition from one mode to another (regions where the TDL modes are jumping rapidly from one mode to another). The noise is caused by competition between the laser modes for the laser power (Harward, 1977), or by a resonance phenomenon between the TDL electron and photon distribution (McCumber, 1966) by a beating between closely spaced transverse modes (Ku, 1977; Harward, 1977). The presence of the noise in the IF causes the blackbody heterodyne signal to be very noisy as evidenced by the upper trace in figure 4. At currents where the IF noise is high or changing rapidly, the heterodyne signal is unusable.

Figures 5 and 6 show mode scans of the TDL taken at a temperature of 21 K. Figure 5 shows the TDL laser modes for the current scans from 0.3 to 1.3 A in 0.1-A steps, while figure 6 shows these mode scans from 1.3 to 1.8 A. The current tuning range of single frequency modes has been considerably reduced.

At this higher temperature, the tuning range of single modes has become so restricted that the TDL is not useful as an LO at the lower currents. The only modes which appear useful for heterodyne purposes are the ones which occur at 10.84 and 10.68 μ for the current ranges 0.9 to 1.3 A and 1.5 to 1.8 A, respectively. Figure 7 shows the 1,000 K blackbody heterodyne signal and excess noise induced by the TDL. This figure was generated in the same manner as figure 4. The TDL appears to be quiet enough for good heterodyne operation for currents less than 0.7 A, but the poor tuning characteristics of the TDL at these lower currents eliminates this set of currents from consideration. The mode noted at 10.8 μ for the set of currents from 0.9 to 1.3 A from figure 5 appears to be a good candidate as a possible LO as is seen from the quiet heterodyne signal and low intergrated IF noise in figure 7 (although even this mode is contaminated by excess noise at the lower current end of its tuning range). The mode at 10.68 μ is not useful since figure 7 shows the 1.5 to 1.8 A current range to be completely dominated by excess noise.

Figures 8 and 9 show the characteristics of the blackbody heterodyne signal and the excess noise for the TDL operating at temperatures of 45 and 70 K respectively. These two curves demonstrate the change in the noise characteristics of the TDL as the temperature increases. In the 45 K case the whole current tuning range of the TDL is dominated by excess noise except for the first 0.15 A after the lasing threshold is reached. For the 70 K curves, the TDL noise characteristics have changed so that much of the current tuning range shows very little excess noise. Therefore, the total tuning range is useful for heterodyne purposes. Mode scans reveal that the TDL operates on only single modes over this tuning range. Thus, the TDL radiation does not need to be passed through a mode selection device thereby increasing the TDL power at the photomixer. The reason for the change in the operating characteristics of this TDL is not well understood at present.

IMPROVEMENTS IN CHARACTERIZATION PROCEDURES

The characterization of the excess noise in the TDL is a very laborious and time-consuming process when the techniques used to obtain the previous characterizations are applied. Even for characteristics taken for every degree kelvin over the TDL operating temperature range, one is never quite sure that all the optimum operating conditions have been determined. Sometimes small changes in either current or temperatures alter the excess noise and/or the spectral character of the TDL. In order to determine the best temperature and current ranges, a real time "picture" of the TDL output needs to be obtained. One way to obtain a real time spectral output of a TDL is to use a rapidly scanning Fabry-Perot etalon. A scanning etalon consists of a pair of flat plates which are maintained parallel. Spectral scans are obtained by displacing one of the plates by applying a voltage ramp to PZT transducers upon which one of the plates is mounted. If the plate is displaced through one-half wavelength, then one free spectral range of elaton is scanned. The free spectral range varies inversely as the spacing between the plates. Thus, in order to determine the spectral output of the TDL, the plates must be spaced such that the free spectral range of the etalon is greater than the range of wavelengths emitted by the TDL at one time.

A spacing of 0.5 mm was chosen for the etalon and was used to obtain real time mode scans. This gave a free spectral range of 10 cm^{-1}, which is just sufficient to cover the TDL emission range (typically 8 to 10 cm^{-1}). Figure 10 shows a real time mode scan obtained for the TDL by scanning the etalon through one free spectral range. The advantage of this technique is that any change in the TDL spectral characteristics can be seen immediately. By observing the oscilloscope screen, one can search for high-intensity wide tuning modes in real time, thereby eliminating much of the time needed to make mode scans with a monochromator. An additional advantage is that any excess noise in a TDL mode can be evaluated simultaneously by observing the integrated IF output of a photomixer on which the etalon-filtered TDL radiation is incident. This is shown in figure 10 by the top negative going trace where both of the TDL modes have generated excess noise on the photomixer. If the integrated IF output shows little or no noise as the etalon is scanned over a TDL mode, then this mode is useful for heterodyne purposes. If the directly detected etalon scan also shows the mode to have a wide tuning range, then it is a good candidate as a possible scanning LO.

This technique has shown good results in that optimum operating conditions can be found more quickly and reliably than the previously used methods. However, there are two disadvantages: the first, and major one, is that the etalon method does not provide the absolute frequency of the TDL modes. This disadvantage can be overcome by making a mode scan in the conventional manner after the optimum operational conditions are found. A second, but minor disadvantage, is that a photograph of the oscilloscope screen provides the only hard copy of the data. With proper instrumentation, this problem can be overcome.

The scanning etalon can be used as a mode isolator in addition to its role as a diagnostic tool. Figure 11 shows the etalon-filtered TDL output as the TDL current is scanned. For this figure the spacing between the etalon plates is held fixed. The upper curve in the figure shows the blackbody heterodyne signal as the TDL scans across the bandpass of the etalon. The lower trace shows the output of a 2.54-cm solid Ge etalon. This trace indicates the spectral half width of the scanning etalon is 0.3 cm^{-1}. The variation in the blackbody heterodyne signal is

directly related to a variation in the transmitted TDL power. These variations make the analysis of the spectra taken with the heterodyne technique very difficult. The problem is removed if the peak of the scanning etalon transmission curve is made to follow the TDL output. This is accomplished by applying a voltage to the external input of the etalon control module which moves the etalon plates to compensate for the TDL spectral change. Such a voltage may be obtained by applying a small dither voltage to the etalon PZT. This causes the transmitted TDL radiation to have a small AC signal impressed on it. This signal is the same frequency as the dither signal. Moreover, this signal changes phase as the TDL output is moved from one side of the etalon transmission curve to the other. At the peak of the etalon transmission curve, the amplitude of the induced AC signal at the dither frequency goes to zero Thus, if a phase-sensitive detector is connected to the bias network of the photomixer, then a voltage proportional to the TDL radiation offset from the etalon peak is obtained. If this voltage is amplified and introduced into the etalon controller, then the etalon transmission peak will be moved to correct for the TDL offset from the etalon transmission peak. Such a feedback circuit is shown in figure 12. The dither signal is applied to the low voltage input of the etalon control unit. The low frequency output of the photomixer on which the TDL radiation is focused is applied to the input to a lock-in amplifier. The feedback loop is completed by connecting the output of the lock-in amplifier to a variable gain voltage amplifier internal to the etalon control module. The sequence for establishing automatic control of the etalon peak is first initiated by manually tuning the DC bias on the etalon control module for maximum transmission of the TDL mode that is to be used. At this point the output of the phase detector should be near zero. When the variable gain on the etalon control module is increased sufficiently, the etalon peak is locked to the wavelength of the TDL.

The advantages of locking the etalon transmission peak over the use of a fixed spaced etalon is seen by comparing figures 13 and 14 with figure 11. Both figures show the same mode used in figure 11, but the etalon is tracking the TDL peak. The tracking etalon has removed the problems shown in figure 11. The temperature was adjusted in figure 14

to increase the tuning range of the TDL. The decrease in the signals at the beginning and end of the current scan in figure 14 was due to the blocking of the TDL. This was done to demonstrate the etalon locking to the TDL wavelength is accomplished in a short time and with little or no overshoot. By counting the Ge etalon fringes in this figure, we see that this mode tuned over approximately a cm^{-1} before cutoff. The full tuning range of this mode cannot be used if either a constant spaced etalon or a conventional monochromator is used for a mode isolation.

This TDL mode isolation technique has direct application in TDL spectroscopy since wider tuning spectral scans can be made, with the additional advantage that the mode isolator profile does not cause power variations in the transmitted TDL radiation. Another advantage which is realized with the tracking etalon technique is the minimization of beam-steering effects. If one uses a monochromator to isolate a single TDL mode beam, then steering effects can cause severe problems. Some of these are uneven intensity fluctuations of the different beams in a multibeam spectroscopic experiment; variation in the calibration of the spacing of the etalon fringes (Flicker et al., 1978) which are sometimes used as relative frequency markers in spectroscopic systems; and longer optical paths which magnify the effects of beam wandering due to thermal misalignment.

SOLAR HETERODYNE MEASUREMENTS

Solar heterodyne measurements were made after the optimum TDL modes were selected. These were accomplished with low-noise (2-dB noise figure), narrow bandwidth (5- to 200-MHz) amplifiers with a 100-MHz low-pass IF filter. Thus the resulting resolution was 200 MHz because of the 2 IF sidebands.

The experimental signal-to-noise ratio (SNR) was determined by beating the TDL with a 1,000 K blackbody. An SNR value of 100 was obtained. The directly detected spectra have a resolution which is in the range from 5 to 30 MHz. Figure 15 shows the similarity between the heterodyne and directly detected resolution. This figure shows three different spectra taken with the TIHR system. These curves were generated with the TDL at

current threshold and cooled to 15 K. The upper two curves show laboratory spectra of HNO_3 for different cell conditions. The top spectrum was taken at a lower HNO_3 partial pressure but with a small amount of air added in order to pressure broaden the spectral lines. The bottom curve shows the heterodyne atmospheric solar absorption spectrum of the same spectral region.

The similarity between the directly detected and solar heterodyne spectra is quite remarkable on two counts. First, each line of the laboratory HNO_3 spectrum correlates with a line in the atmospheric absorption spectrum. Second, the low-pressure broadened HNO_3 has the same appearance as the atmospheric absorption spectra. Not only do these spectra match each other, they also match synthetic HNO_3 spectra obtained from spectroscopic parameters. In fact, the number scale on this figure was obtained from the theoretical positions. Not all of the lines in the atmospheric spectra match HNO_3 lines, and these are due to absorption by other atmospheric species. The strong absorption feature in the solar heterodyne measurement is attributed to CO_2 and H_2O. Figures 16 and 17 show simulated atmospheric spectra generated from the line parameters and assumed profiles for HNO_3, CO_2, and H_2O. The difference in these two figures is due to different assumed vertical concentration profiles of H_2O, where figure 16 has one-half the assumed water vapor content in figure 17. If the power change in the TDL is taken into account, the experiment and synthetic absorption spectra compare quite nicely. No attempt has been made to optimize the fit, since the experimental spectrum was not normalized for the TDL power variations, nor was the heterodyne system calibrated to determine the absolute solar intensity.

Figure 18 shows the heterodyne atmospheric solar absorption spectra obtained with the TDL temperature at 69.9 K. At this temperature the TDL operates in single modes for the currents used. This is evidenced by the examination of the etalon traces in the lower part of the figure. Each of the modes tunes over approximately 0.5 cm^{-1} as indicated by the number of etalon fringes (spaced 1.5 GHz apart). The cause of the excess noise seen at the beginning of region G is not precisely known, but it is probably due to very small transverse modes which are in competition

for the TDL power. For currents higher than the ones used, the TDL output definitely becomes multimode with an excess of noise. The letters at the bottom of the figure indicate different spectral regions shown in high resolution in Fourier Transform Spectrometer (FTS) scans of solar radiation (Goldman et al., 1978). These marked regions show the TDL single-mode regions and are shown again in figures 19 and 20. The absorption is caused by ozone, carbon dioxide, and water vapor. The absorption in different parts of the atmosphere is evidenced in figure 18 by the width of the absorption lines. The lines caused by absorption in the stratosphere are very narrow (doppler broadened) while absorption in the lower atmosphere results in wider lines (collision broadened). This is demonstrated by region E in figure 18, where the stratosphere ozone lines are superimposed on the CO_2 absorption line. The spectra seen in this figure represent the highest resolution atmospheric spectra obtained to date. The resolution here is approximately 0.006 cm^{-1} and is 10 times better than high resolution (0.06 cm^{-1}) FTS spectra. In fact the FTS spectra resolution are just a little less than the distance between the etalon fringes.

Figure 21 and 22 show atmospheric absorption spectra obtained with the TDL operating at 70.3 K. The spectral regions covered in these figures are different from the ones obtained at 69.9 K. Figure 21 was obtained by scanning the TDL-injection current in a positive manner, while figure 22 was obtained by scanning the current from high currents toward lower values. Close examination of the same lettered regions shows that two different spectral regions are observed when scanning in this manner. Mode-pulling effects are responsible for these differences. Once a mode begins to lase, that mode will lase at current lower than the threshold current for that mode. Hence, the mode will lase at different wavelengths depending on the direction of the current scan. Therefore, at each of the temperatures used, the current was scanned in both manners in order to increase the spectral coverage. Figures 23 and 24 show atmospheric spectra obtained at 70.6 K for the forward and reverse current scans respectively. We see that the temperature change causes the modes to cover a slightly different spectral region. Figure 25 shows the spectrum obtained at 70.9 K with the current scanned in

the reverse direction. No forward-direction current scan was obtained at this temperature. Two new spectral regions are obtained at this temperature, i.e. regions L and M. Figures 26 and 27 show the spectra obtained at 71.3 K with current scans in the forward and reverse current directions respectively. Figure 28 and 29 show atmospheric spectra obtained at 72 K for forward and reverse current scans. The ordinate in the figure is expanded over previous ones. This illustrates the spectra better, but of course it does reduce the number of spectral regions covered in one scan.

Figures 30 and 31 show the atmospheric spectra obtained at 72.5 K for a current scan in the forward and reverse directions respectively. Figure 32 shows the current scan in the reverse direction with the TDL temperature at 73 K.

This scan includes a new spectral region. Table 1 gives the approximate wave number range of the lettered regions and atmospheric species which cause the absorption. The main absorbing species are CO_2 and H_2O in the lower atmosphere and O_3 in the stratosphere. While these scans of the atmospheric spectra are quite encouraging, they are not useful in a practical sense. This is because of the condensed nature of these spectral scans. If the single mode regions are expanded, then the scans will show the finer details of the atmospheric spectra. Figure 33 and 34 show the atmospheric absorption spectra with expanded scales. These scans were obtained with the single-mode region labeled K in the previous figures. The increase in the detail is evident in figures 33 and 34 which were obtained with forward and reverse current scans. The mode-pulling effects in these two spectra are prominent. The region L is wider in figure 33 than in figure 34, due to a lower wavelength in the forward current scan than in the reverse scan.

Differences in the appearance of the absorption lines are related to the environment where the absorption took place. The broad absorption line is due to absorption by CO_2, which takes place primarily in the lower atmosphere. The narrow lines are attributed to absorption by ozone in the stratosphere. This difference in the shape of the absorption

Table 1. Approximate wave number range of the lettered regions and atmospheric species which cause the absorption.

REGION	WAVE NUMBER RANGE (cm^{-1})	ABSORBING SPECIES
A	1064 - 1064.6	O_3
B	1066.2 - 1067.1	O_3, CO_2, H_2O
C	1068.3 - 1069.4	O_3, CO_2
D	1070.9 - 1071.7	O_3
E	1072.8 - 1073.7	CO_2, O_3
F	1075.0 - 1076.0	O_3, H_2O
G	1077.4 - 1078.2	O_3, CO_2
H	1079.4 - 1080.2	O_3, CO_2
I	1081.8 - 1082.5	CO_2, O_3
J	1084.2 - 1085.0	CO_2, O_3
K	1086.5 - 1087.2	CO_2, O
L	1088.7 - 1089.3	O_3, CO_2
M	1091.2 - 1091.8	H_2O, O_3
N	1092.7 - 1093.2	O_3

lines caused by pressure broadening is exploited in heterodyne systems to give profiles of atmospheric species.

Before the atmospheric spectra taken with the TIHR can yield quantitative information about the atmospheric profiles, several refinements need to be made to the system. The first refinement is the inclusion of a phase-sensitive amplifier locked to the solar beam chopper. Input of this phase detector would be connected to the DC bias supply of the photomixer. This would enable us to measure the amount of chopped solar-induced shot noise. This chopped noise gives rise to a false signal from the IF amplifiers, and the signal appears as a positive offset in the heterodyne signal since the chopped heterodyne signal has the same phase relative to the chopper as does the solar-induced shot noise. Since the very low frequency component of the solar shot noise should be proportional to the higher frequency components, the offset in the heterodyne signal can be corrected by measuring the low frequency component.

A second refinement to the system is needed to correct for the proportionality between the TDL power and the heterodyne signal. This proportionality accounts for some of the variation in the magnitude of the heterodyne signal. The effect can be corrected for by measuring the TDL power on the photomixer. One method would mechanically chop the TDL beam, but this diminishes the heterodyne signal by a factor of 2 (because of the 50 percent duty cycle of conventional choppers). Since the level of the heterodyne signal is already small, this method would not be acceptable. Another method involves the use of the mode-isolating etalon. In this method a 10 percent duty cycle pulse is added to the bias voltage of the etalon. If the level is sufficient, then the peak of the etalon transmission will move away from the TDL emission frequency (assuming the etalon is tracking the TDL mode). Thus the TDL radiation will effectively be chopped with only a 10 percent off time. The TDL power is then synchronously detected with either a lock-in amplifier or a boxcar average resulting in only a 10 percent reduction in the heterodyne signal.

The volume of data that can be generated by the TIHR is tremendous: too much so for hand processing or recording only in the form of x-y

plots. Thus a third and final addition to the present system would be an automatic data acquisition system for taking the data and storing on magnetic tape for later processing.

CONCLUSIONS

A tunable infrared heterodyne radiometer which uses a diode laser as the local oscillator has been described. Methods for the evaluation of the noise characteristics of the TDL for their use as local oscillators have been described and discussed. The relative merits of the different TDL mode isolation schemes have also been discussed with the conclusion that the tracking etalon offers the best characteristics for this task. Preliminary atmospheric absorption data has been presented which shows the capability of the TIHR for making the highest resolution atmospheric measurements to date. Atmospheric spectra have been shown for HNO_3, H_2O, CO_2, and O_3. The ability of the TIHR to measure the profiles of different atmospheric species has been pointed out, but refinements need to be made to the system before these profiles can be obtained on a regular basis.

ACKNOWLEDGMENTS

We wish to thank the personnel of NASA/Langley Research Center's Laser and Spectroscopy Branch for their cooperation in allowing this work to be accomplished. Additionally we thank Dr. Wayne Lo of General Motors Research Laboratory for loan of the lead salt laser used in this work.

REFERENCES

Flicker, H.; Aldridge, J.P.; Filip, H.; Nereson, N.G.; Reisfeld, M.R.; and Weber, W.H.: Wavenumber Calibration of Tunable Diode Lasers Using Etalons. Appl. Phys., Vol. 17, 1978, p. 851.

Frerking, M.A.; and Muehlner, D.J.: Infrared Heterodyne Spectroscopy of Atmospheric Ozone. Appl. Opt., Vol. 16, 1977, p. 526.

Goldman, A.; and Blatherwick, R.D.: Analysis of High Resolution Solar Spectra in the 2.5 to 15 μm Region. Annual Report prepared under Grant ATM 76-83908, The National Science Foundation, 1978.

Hackett, C.E.: A tunable Diode Laser Heterodyne Spectrometer for Balloon-Borne Solar Radiometry in the Stratosphere. Sandi Laboratories (Albuquerque, NM), Technical Report SAND 77-0601, 1977.

Harward, C.N.: The Evaluation of a HgCdTe Photomixer with a Tunable Diode Laser (TDL) and the Evaluation of TDL's as a Local Oscillator in a Heterodyne Detection System. Final Report for NASA Grant NSG 1197, Nov. 1977.

Ku, R.T.; and Spears, D.L.: High-Sensitivity Heterodyne Radiometer Using a Tunable Diode Laser Local Oscillator. IEEE/OSA Conference of Laser Engineering and Applications (Washington, DC), June 1-3, 1977.

McCumber, D.E.: Intensity Fluctuations in the Output of CW Laser Oscillators I. Phys. Rev., Vol. 141, 1966, p. 306.

Mumma, M; Kostiuk, T.; Cohen S.; Buhl, D.; and von Thuna, P.C.: Infrared Heterodyne Spectroscopy of Astronomical and Laboratory Sources at 8.5 μm. Nature, Vol. 253, 1975, p. 514.

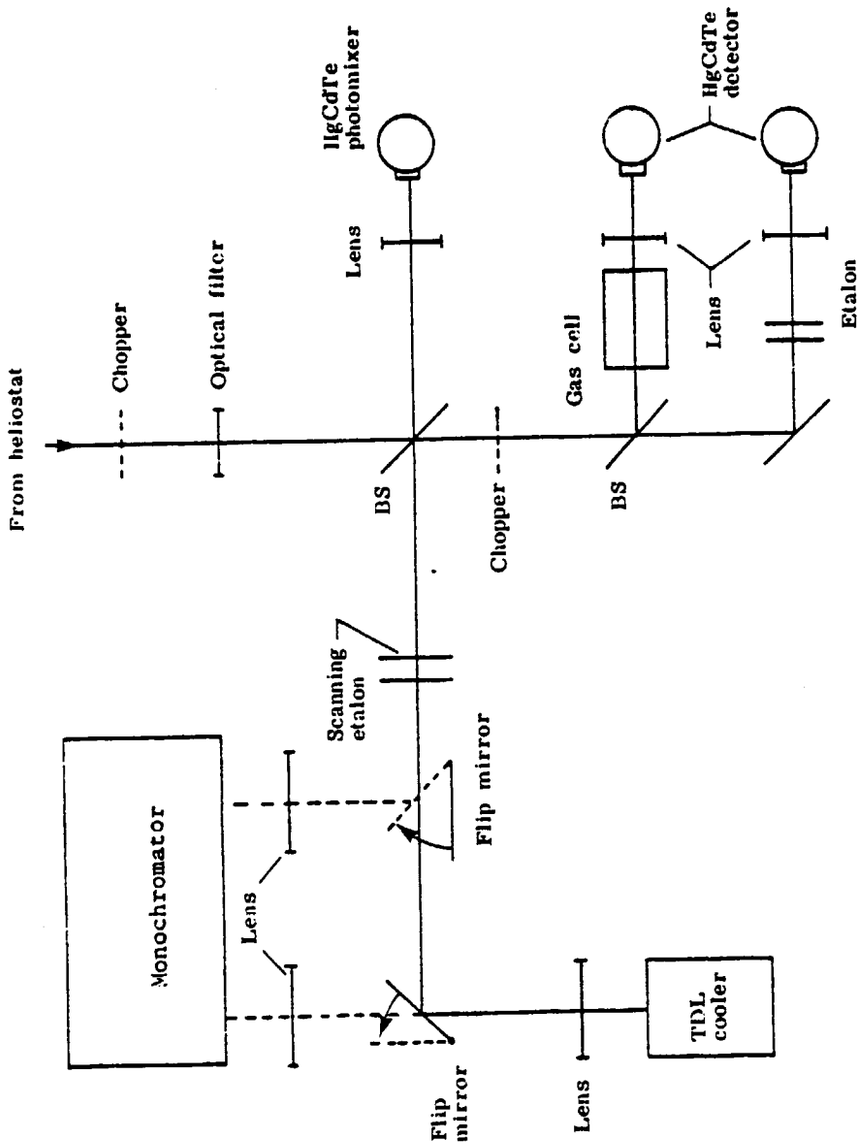

Figure 1. Optical schematic for heterodyne radiometer.

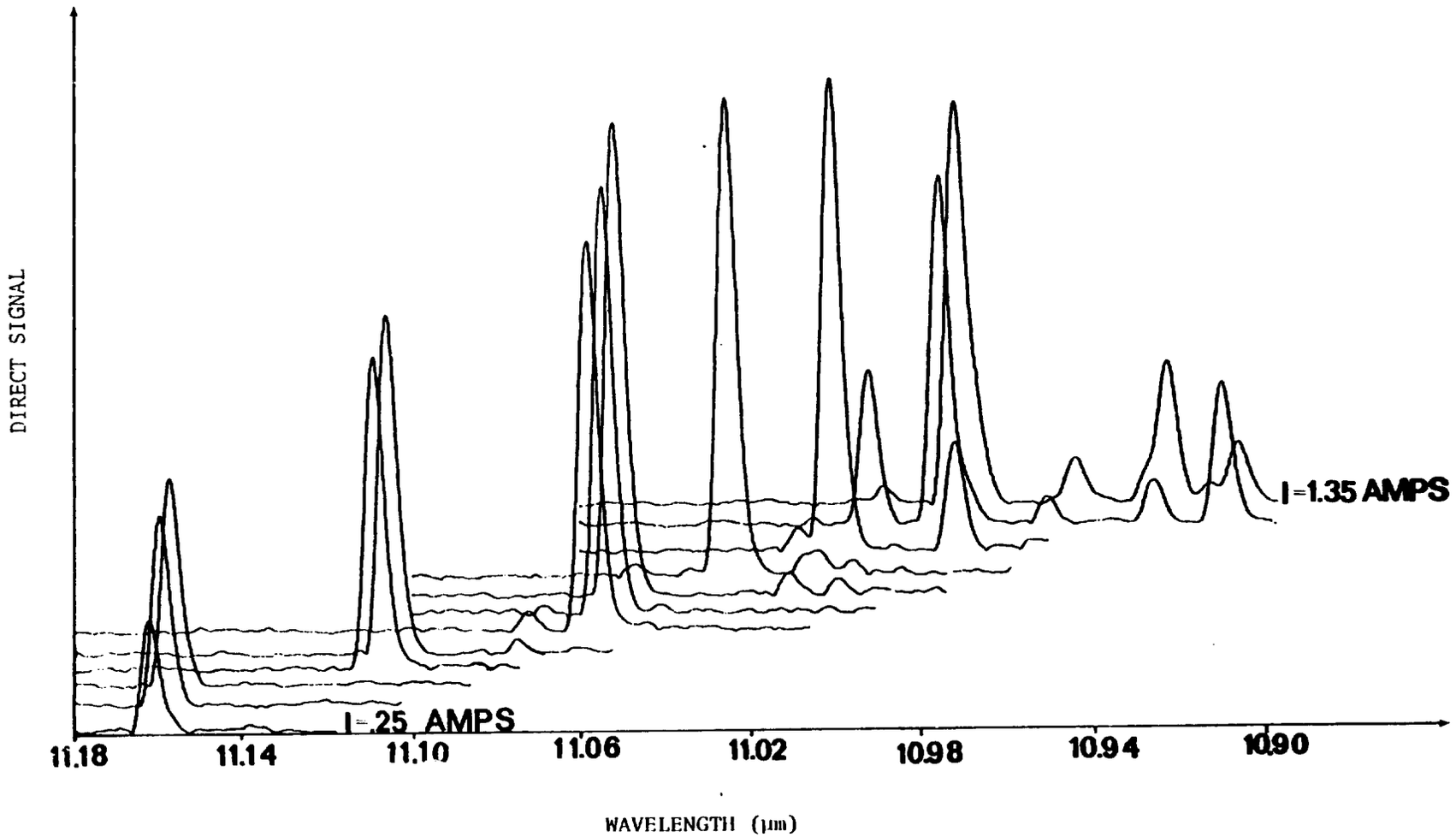

Figure 2. TDL mode scans for currents from 0.25 to 1.35 A at 16 K.

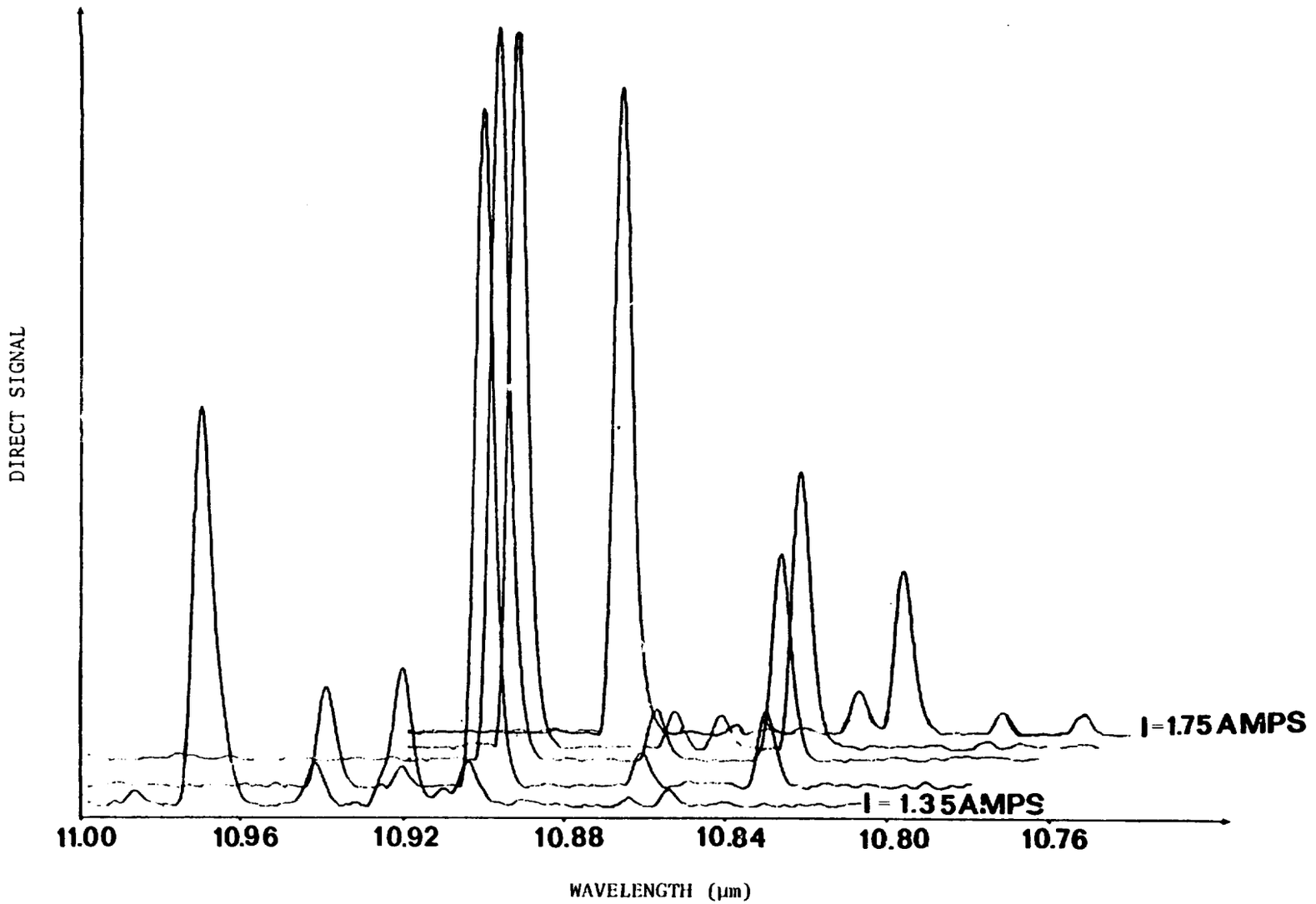

Figure 3. TDL mode scans for currents from 1.35 to 1.75 A at 16 K.

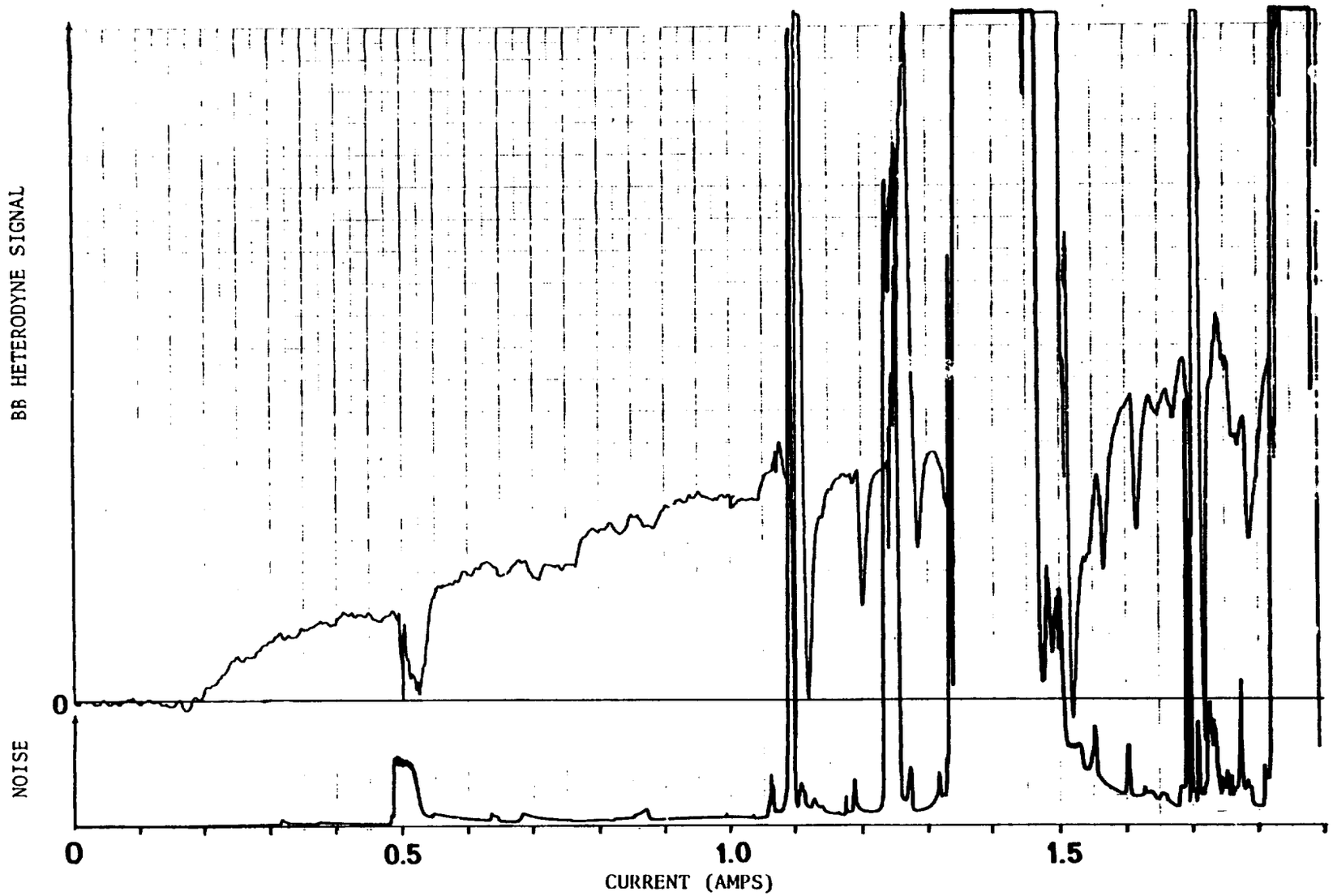

Figure 4. 1,000 K blackbody heterodyne signal and TDL-induced excess noise at 16 K for currents up to 1.9 A.

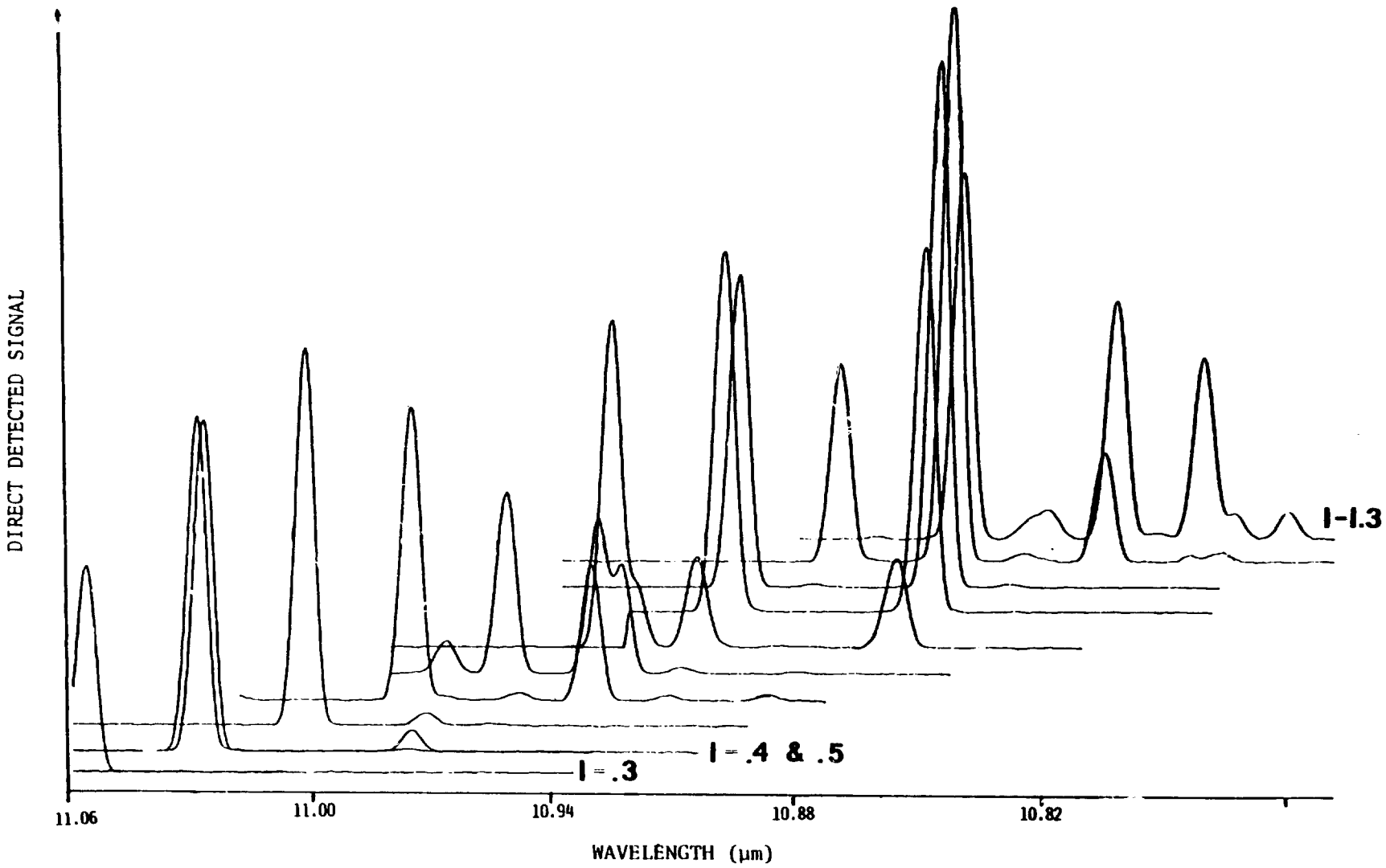

Figure 5. TDL mode scans for currents from 0.30 to 1.30 A at 21 K.

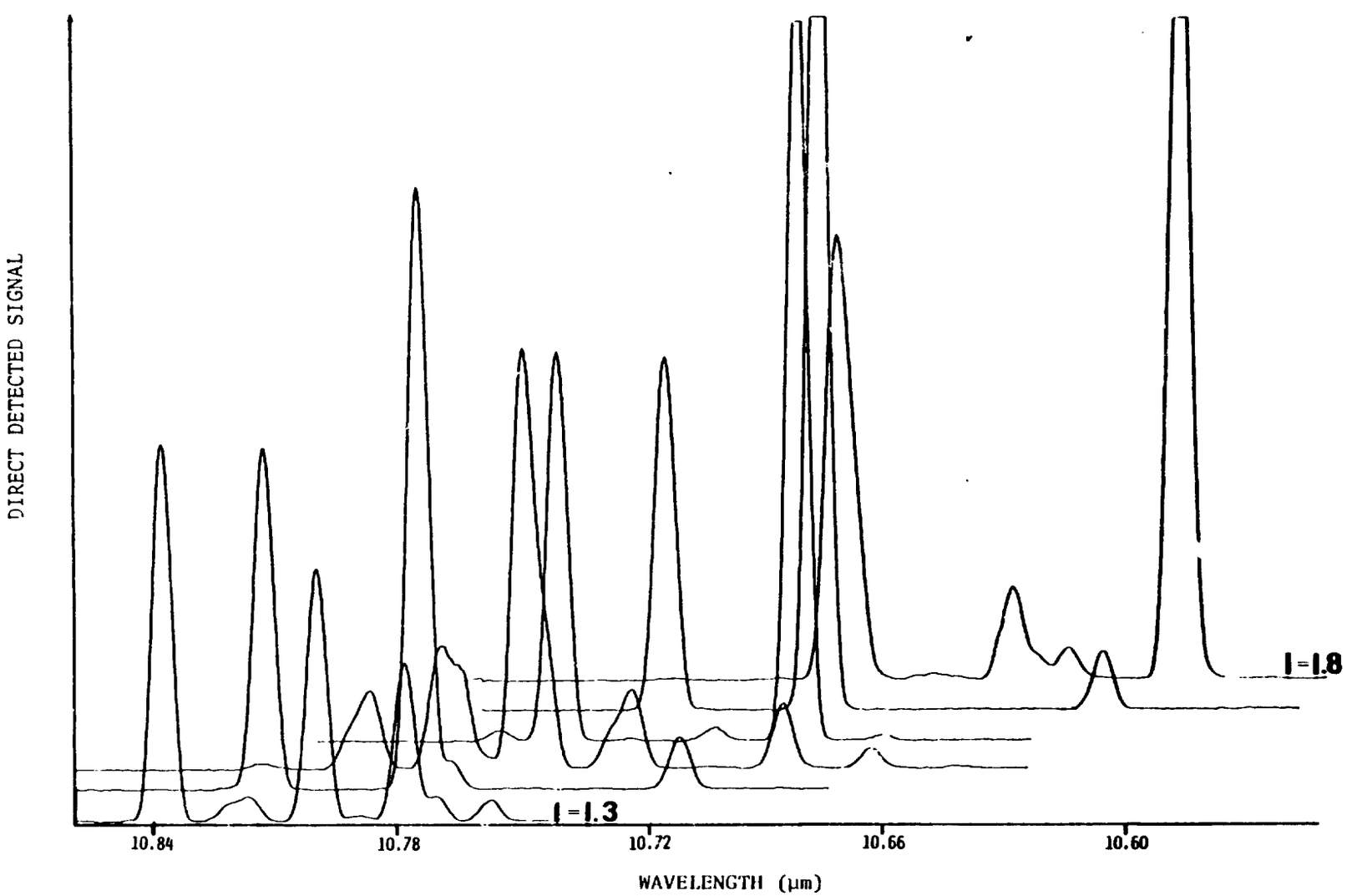

Figure 6. TDL mode scans for currents from 1.30 to 1.80 A at 21 K.

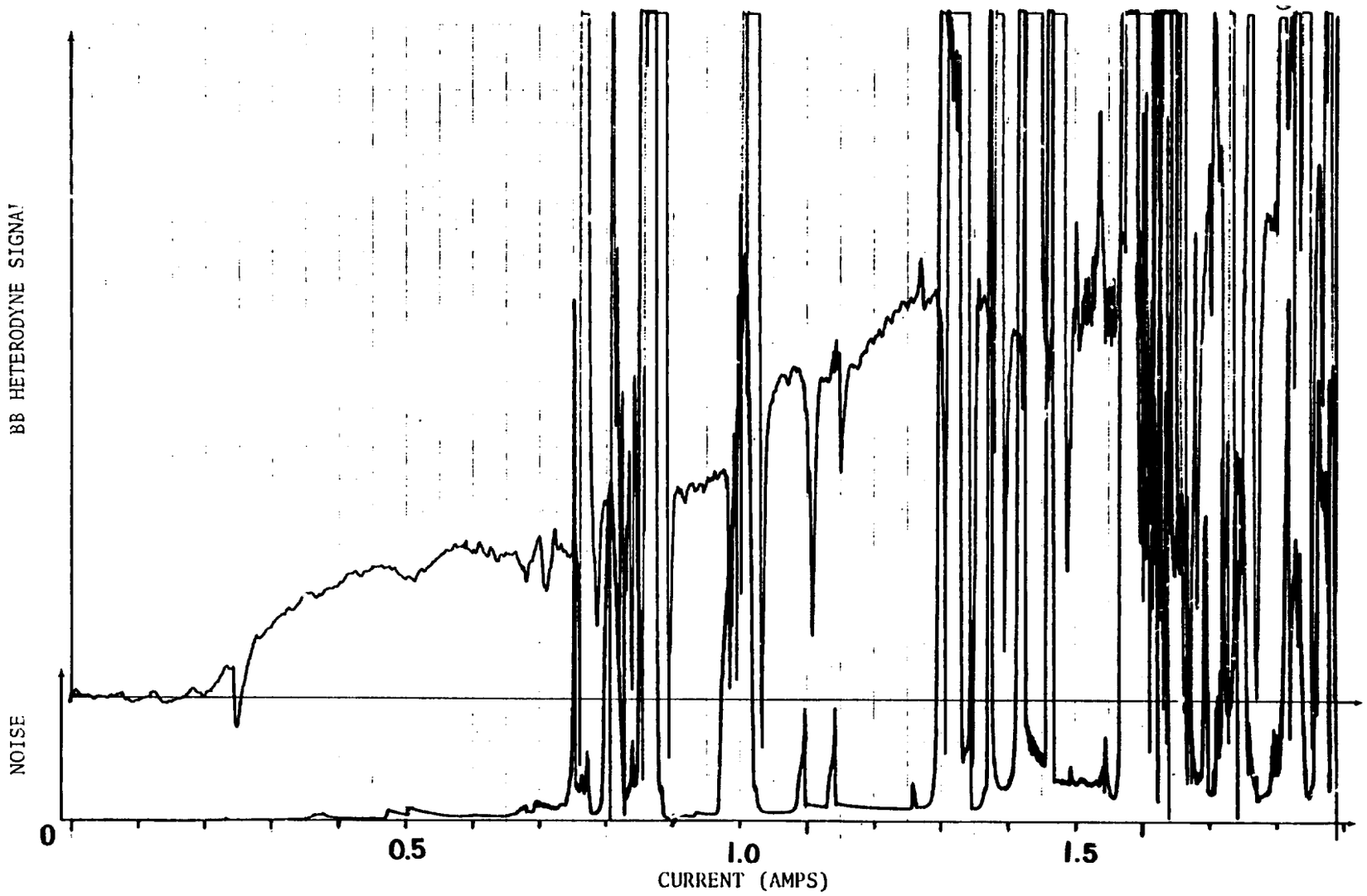

Figure 7. 1,000 K blackbody heterodyne signal and TDL-induced excess noise at 21 K for currents up to 1.90 A.

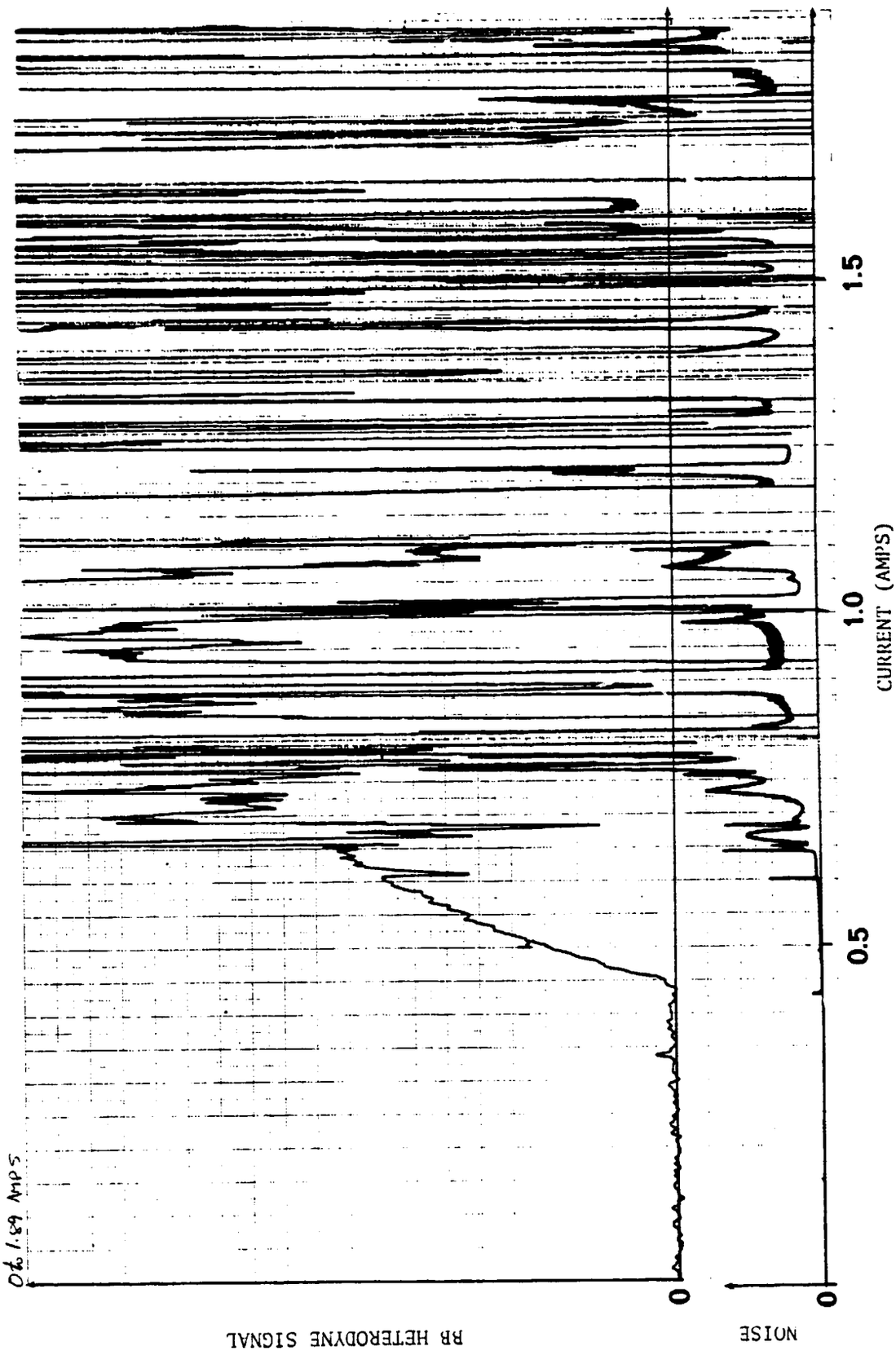

Figure 8. 1,000 K blackbody heterodyne signal and TDL-induced excess noise at 45 K for currents up to 1.90 A.

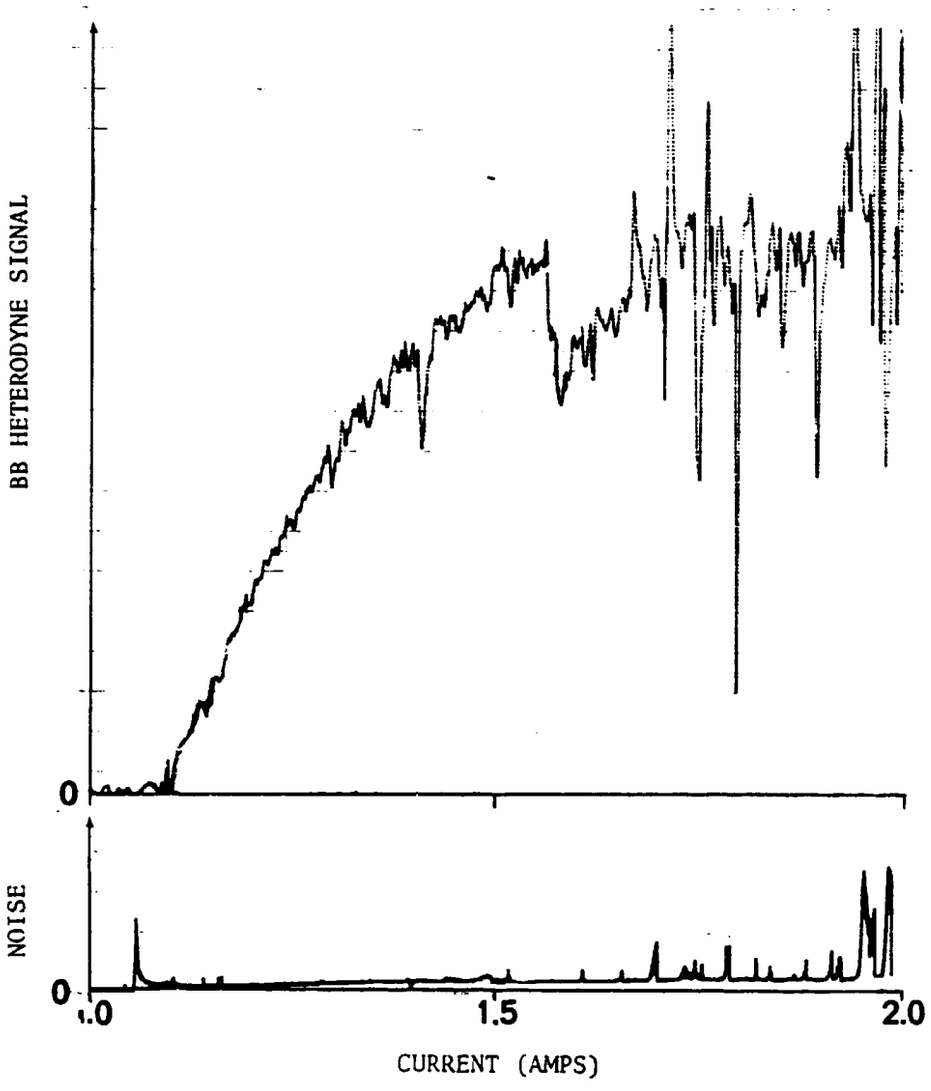

Figure 9. 1,000 K blackbody heterodyne signal and TDL-induced excess noise at 70 K for currents up to 1.90 A.

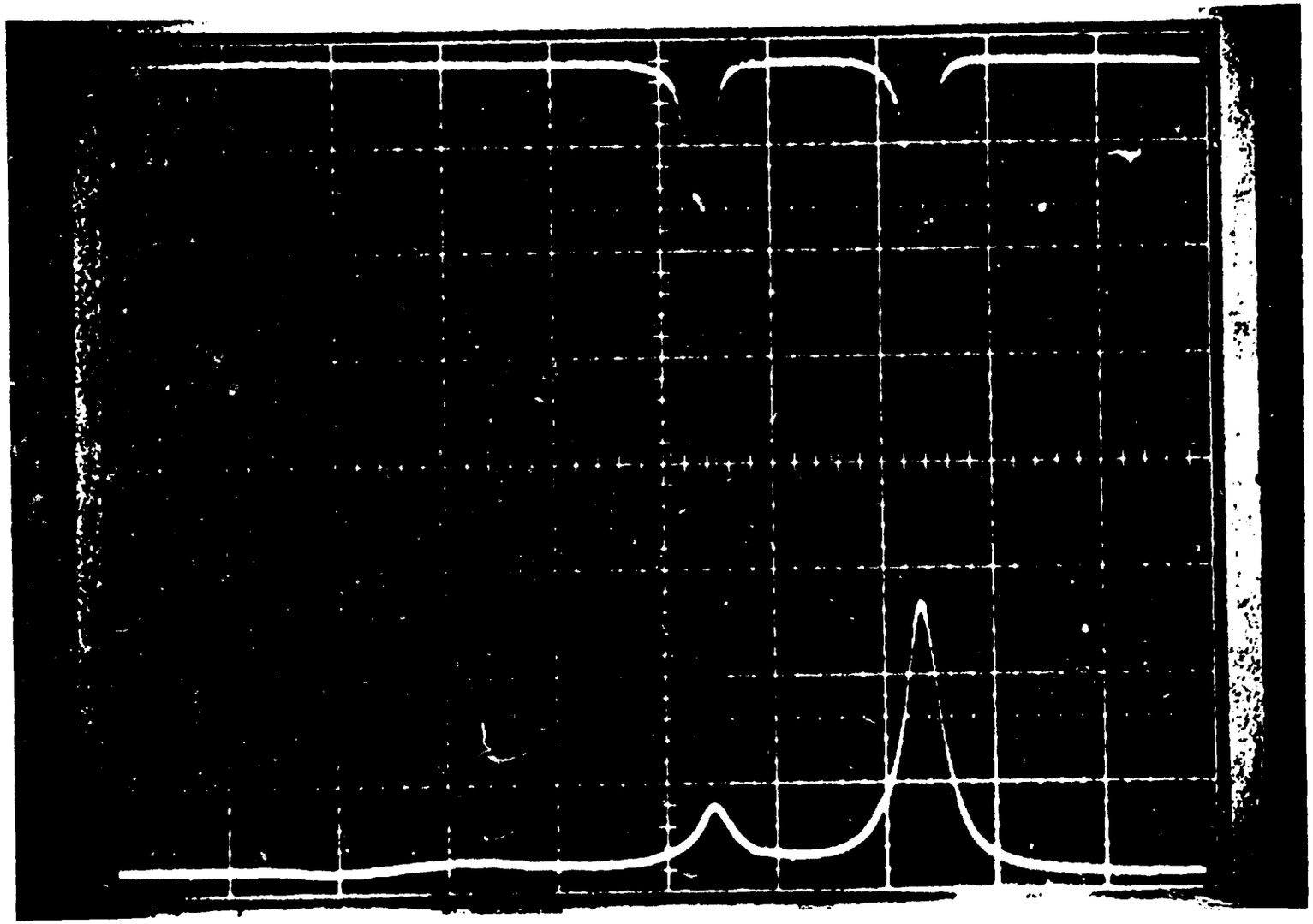

Figure 10. Real time etalon scan of TDL modes (bottom trace) along with excess noise associated with TDL modes (top trace). Noise is increasing in downward direction.

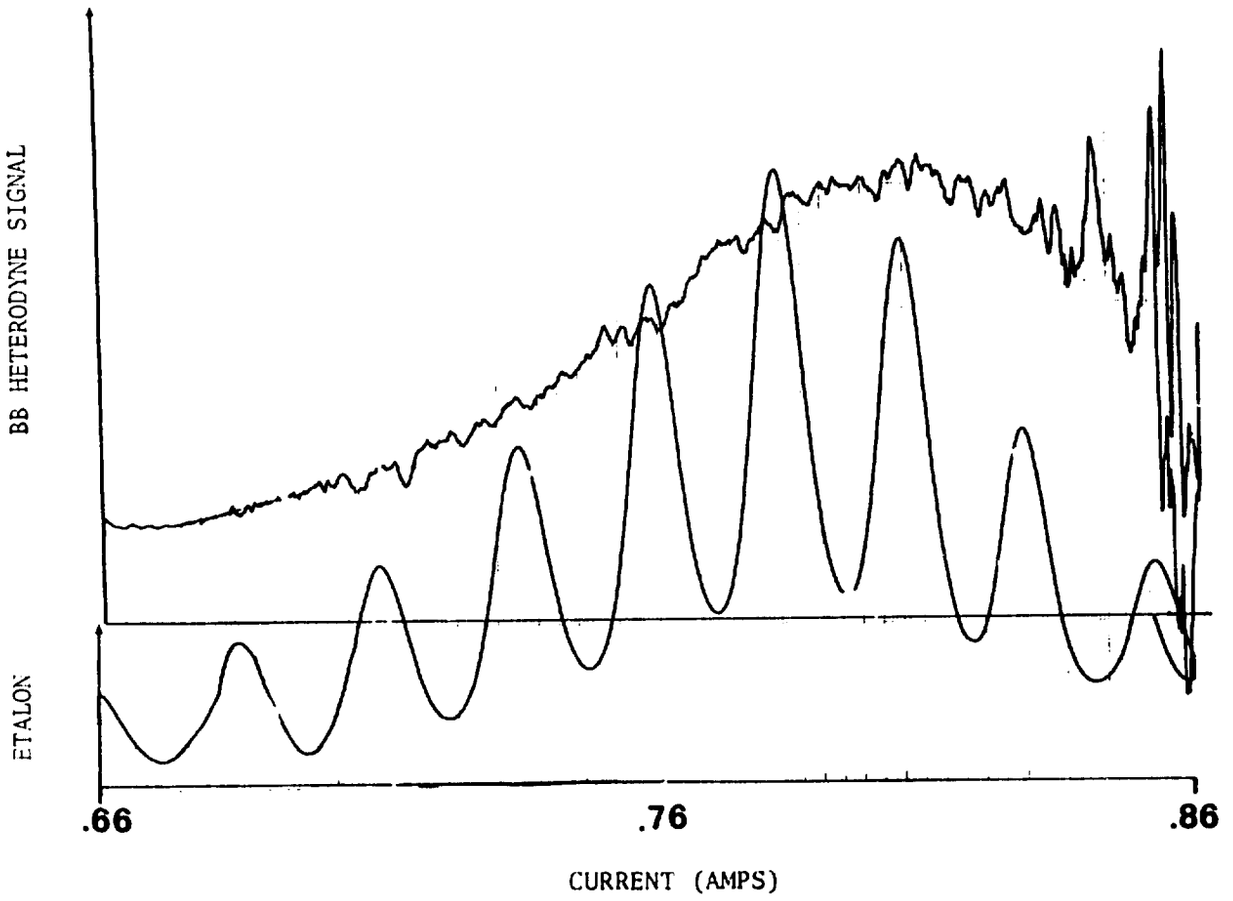

Figure 11. Single-mode 1,000 K blackbody heterodyne signal obtained with fixed space etalon as a mode isolator (top trace). Bottom trace shows the output of a 2.54-cm solid Ge etalon.

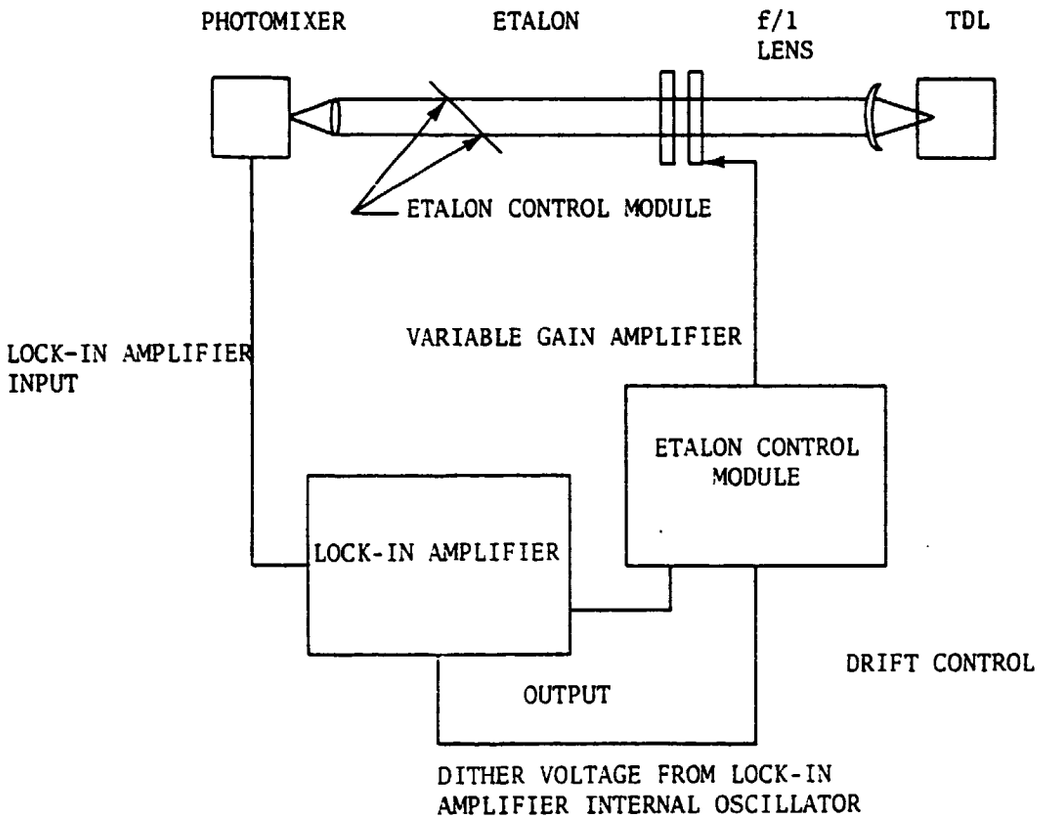

Figure 12. Tracking control circuit for etalon.

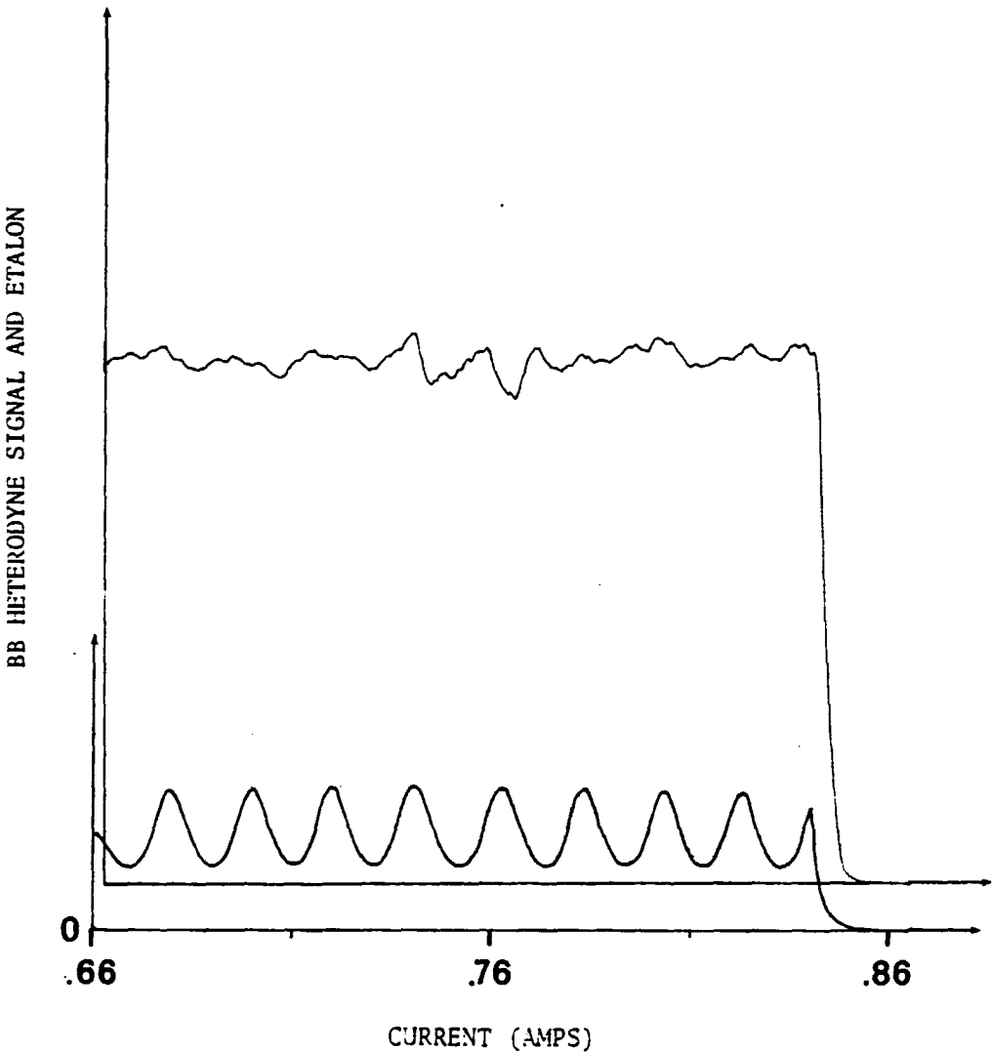

Figure 13. Single mode 1,000 K blackbody heterodyne signal obtained with etalon peak locked to the TDL wavelength. Bottom trace shows the output of a 2.54-cm Ge etalon.

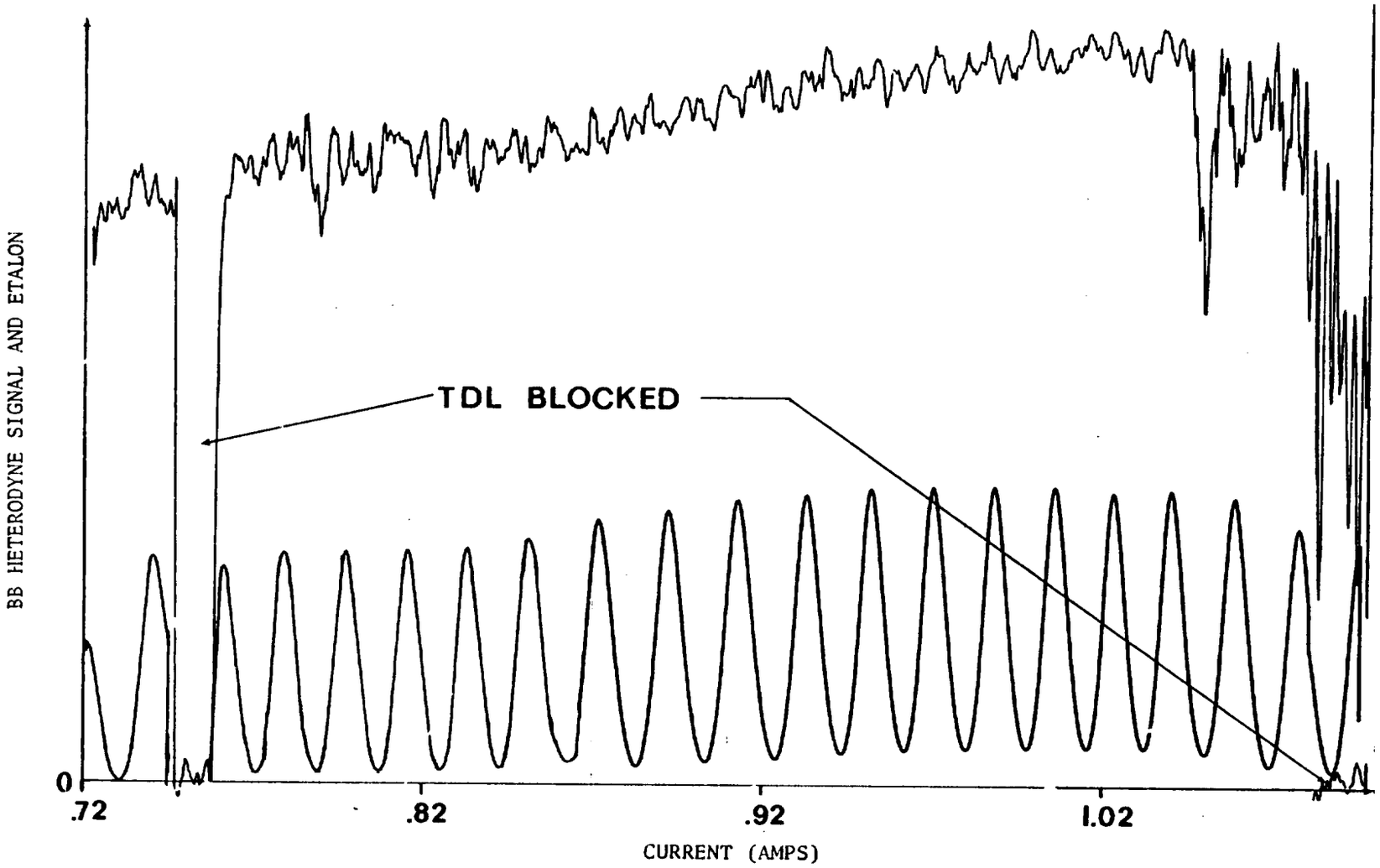

Figure 14. Single-mode 1,000 K blackbody heterodyne signal obtained with etalon peak locked to the TDL wavelength. Bottom trace shows the output of a 2.54-cm Ge etalon. Temperature adjusted from figure 13 to increase the tuning range of TDL.

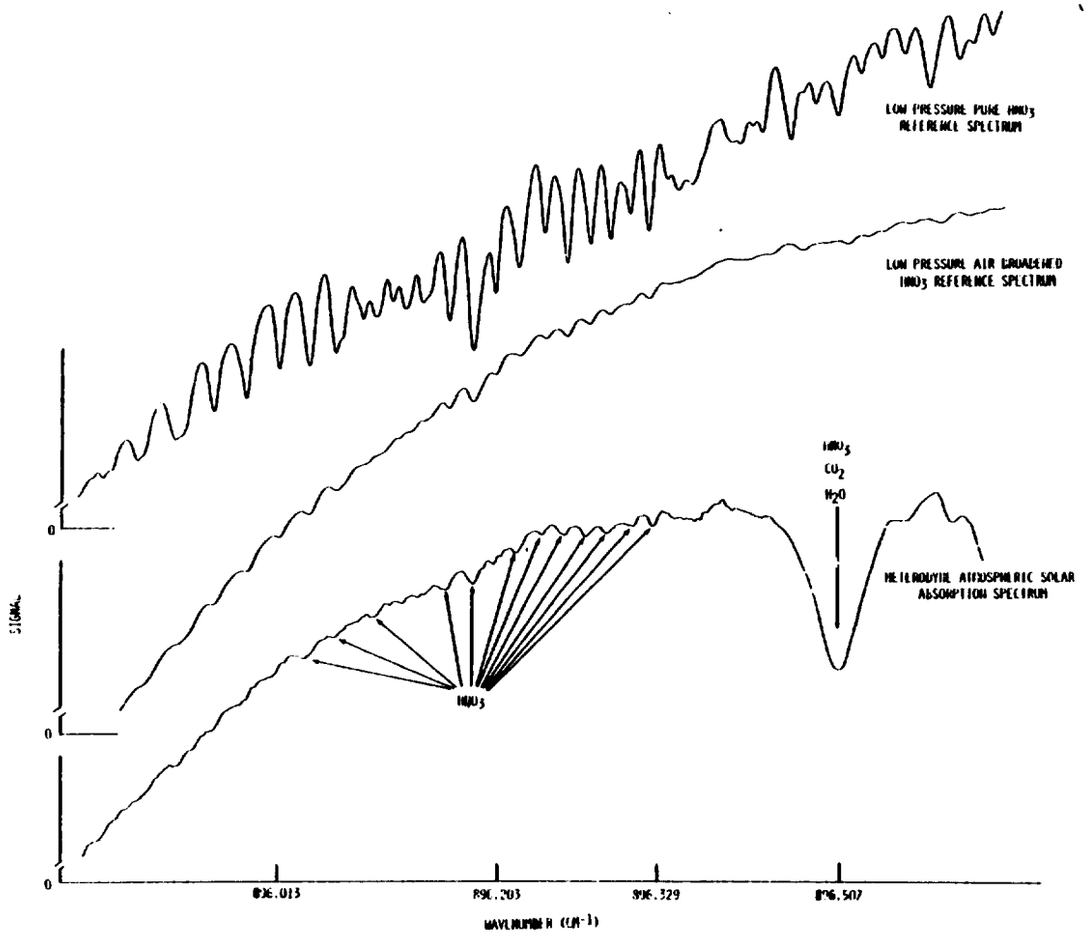

Figure 15. Heterodyne atmospheric solar absorption spectrum along with directly detected HNO_3 spectrum.

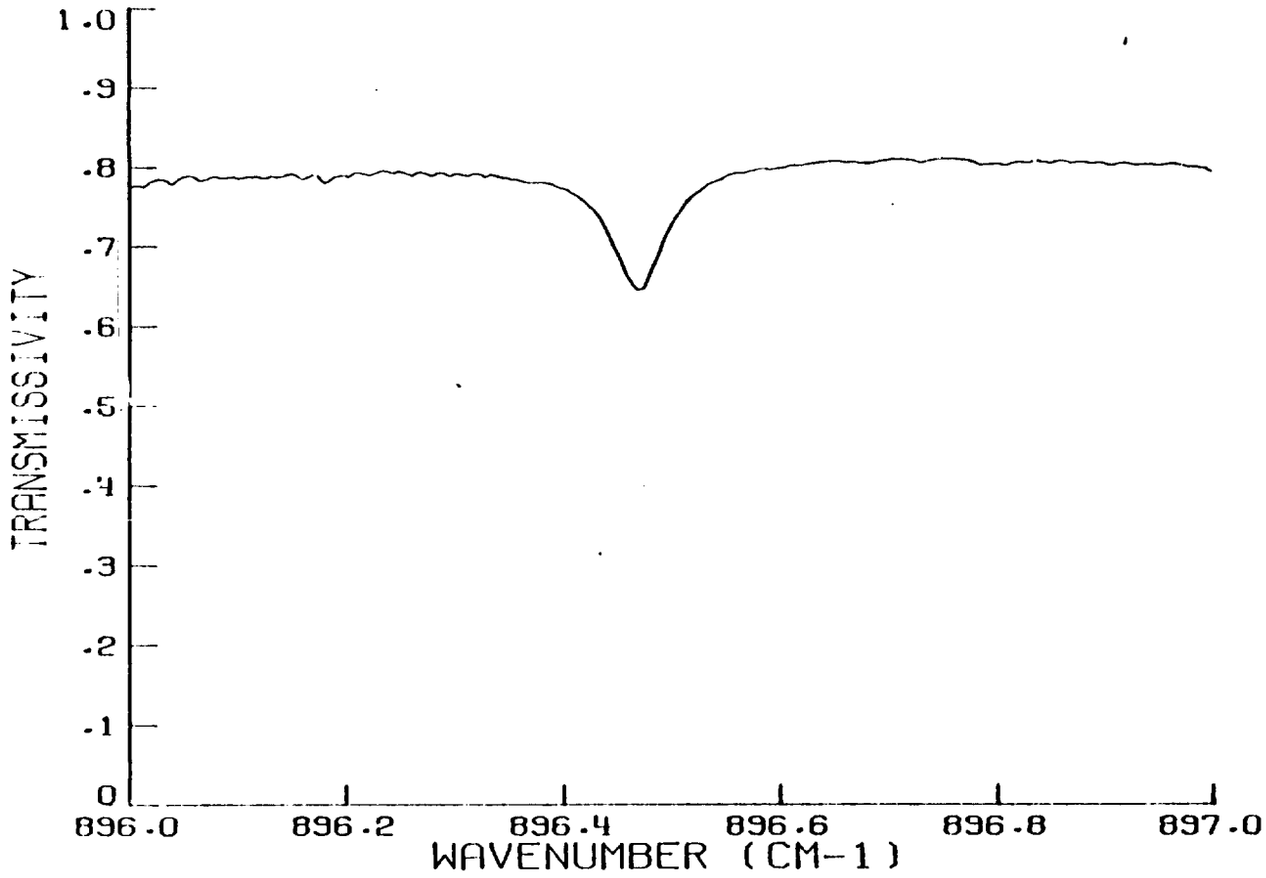

Figure 16. Simulated atmospheric spectrum generated from the line parameters and assumed profiles for HNO_3, CO_2, and H_2O.

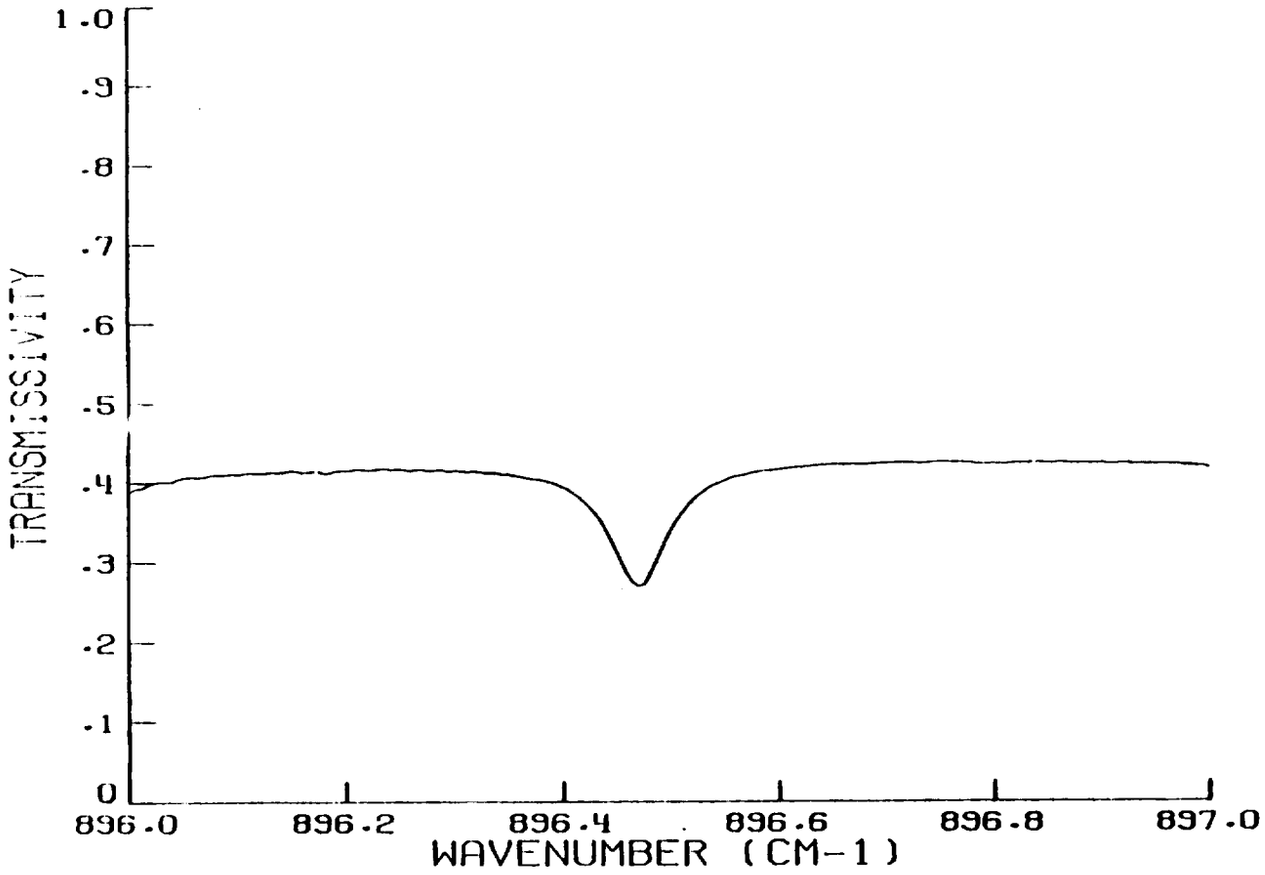

Figure 17. Simulated atmospheric spectrum generated from the line parameters and assumed profiles for HNO_3, CO_2, and H_2O. H_2O content is one-half that of figure 16.

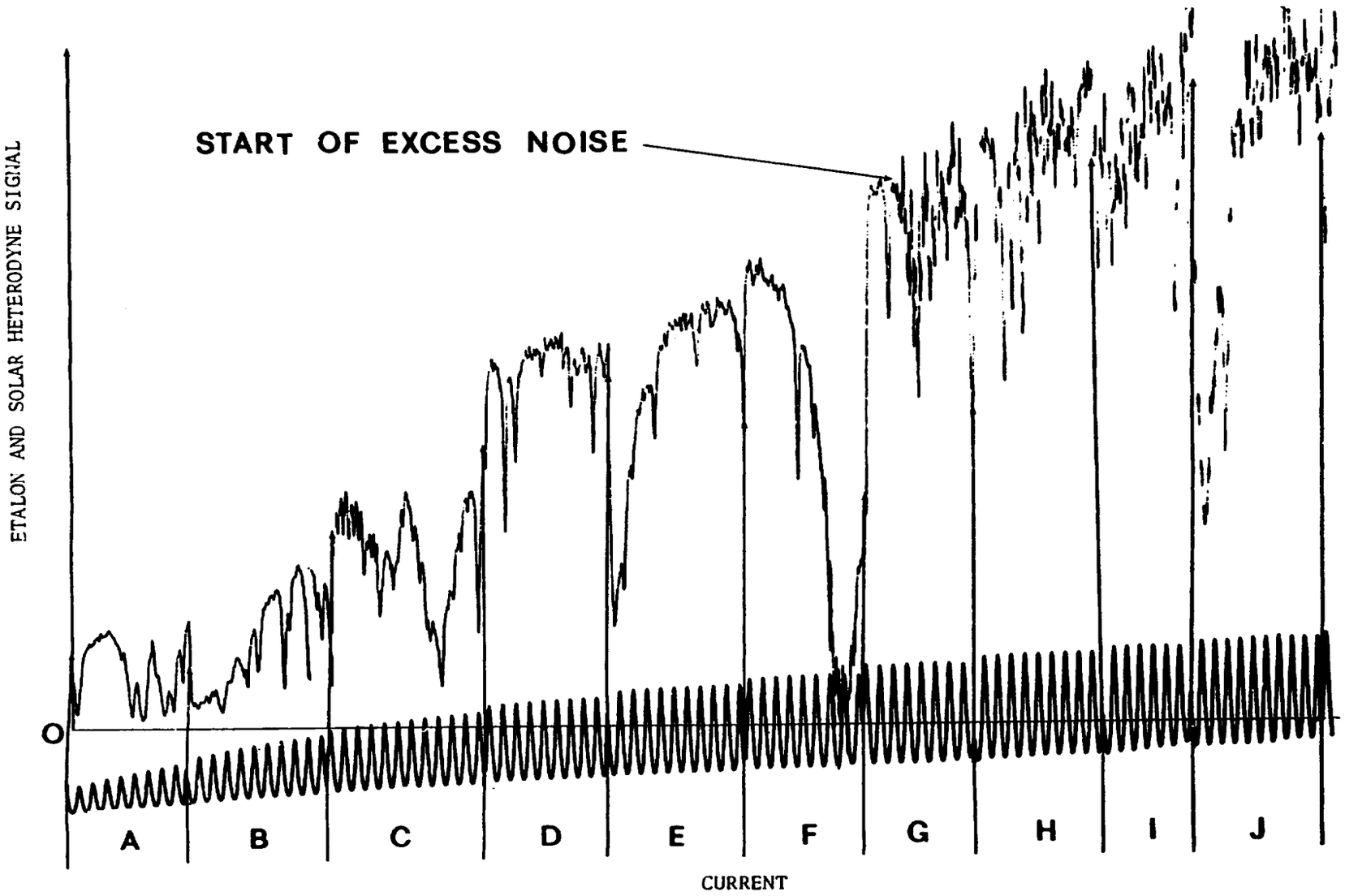

Figure 18. Heterodyne atmospheric solar absorption spectra along with etalon fringes obtained with the TDL temperature at 69.9 K.

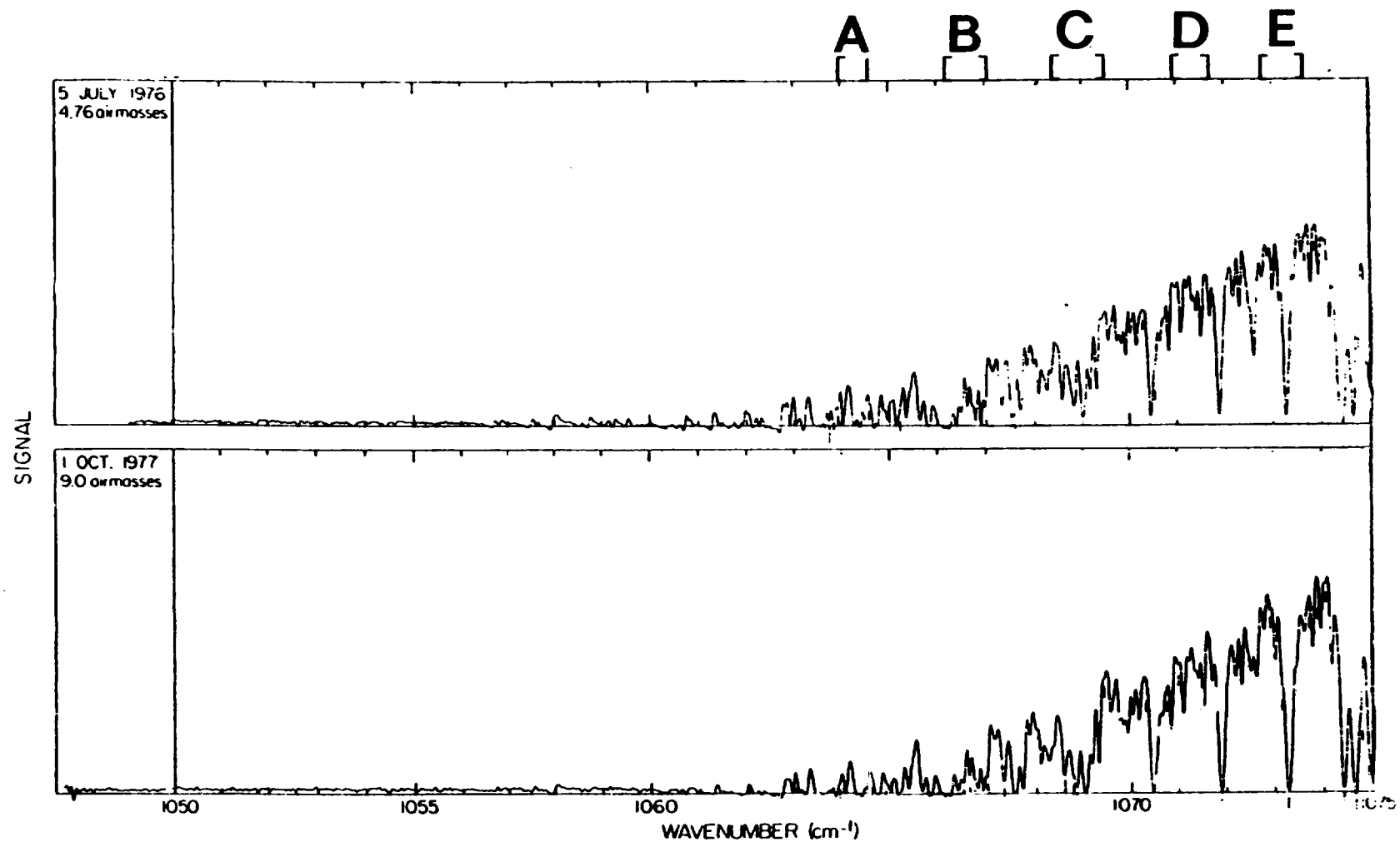

Figure 19. Fast Fourier transform atmospheric spectra from 1,050 to 1,075 cm^{-1} (Goldman et al., 1978).

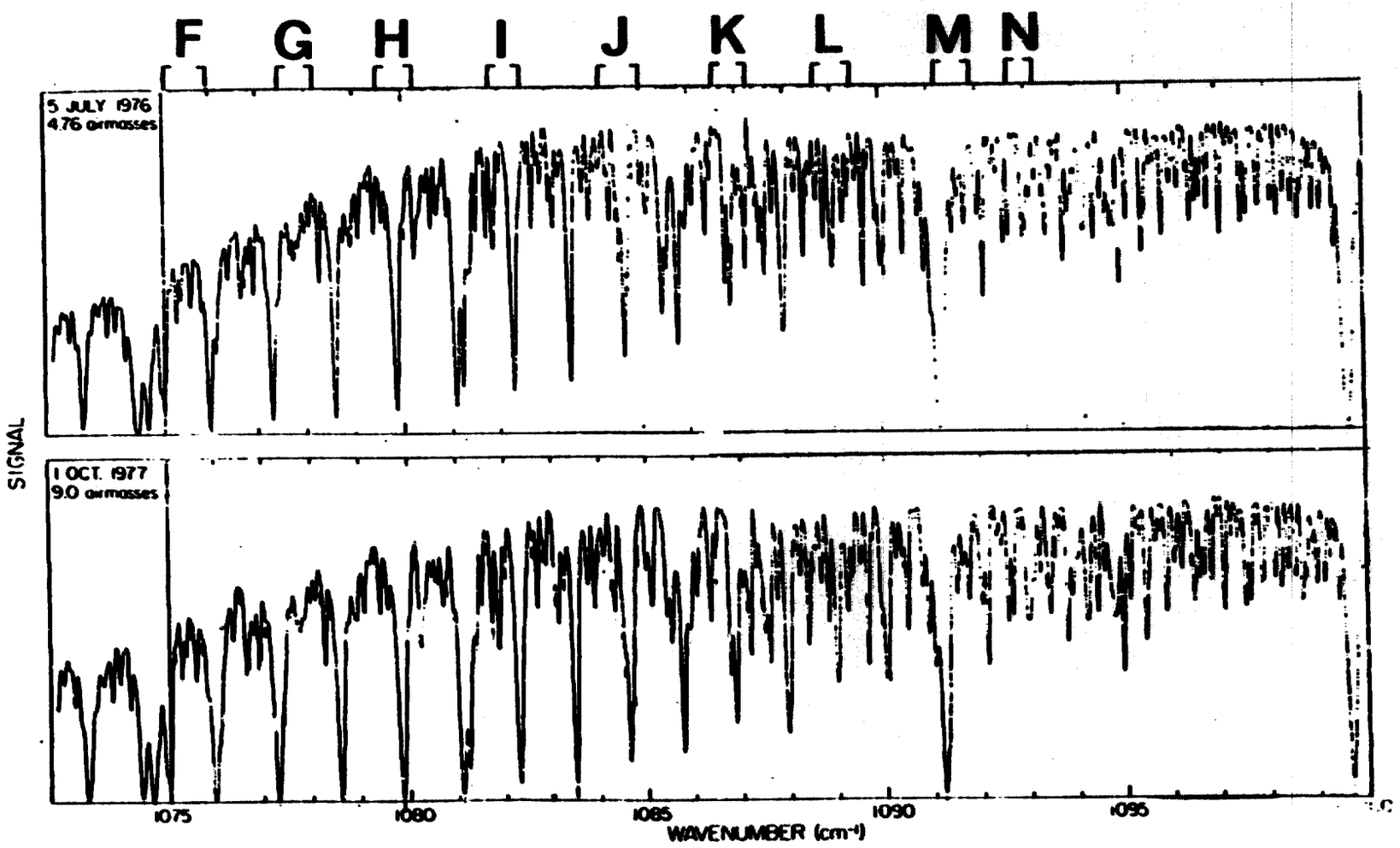

Figure 20. Fast Fourier transform atmospheric spectra from 1,075 to 1,100 cm^{-1} (Goldman et al., 1978).

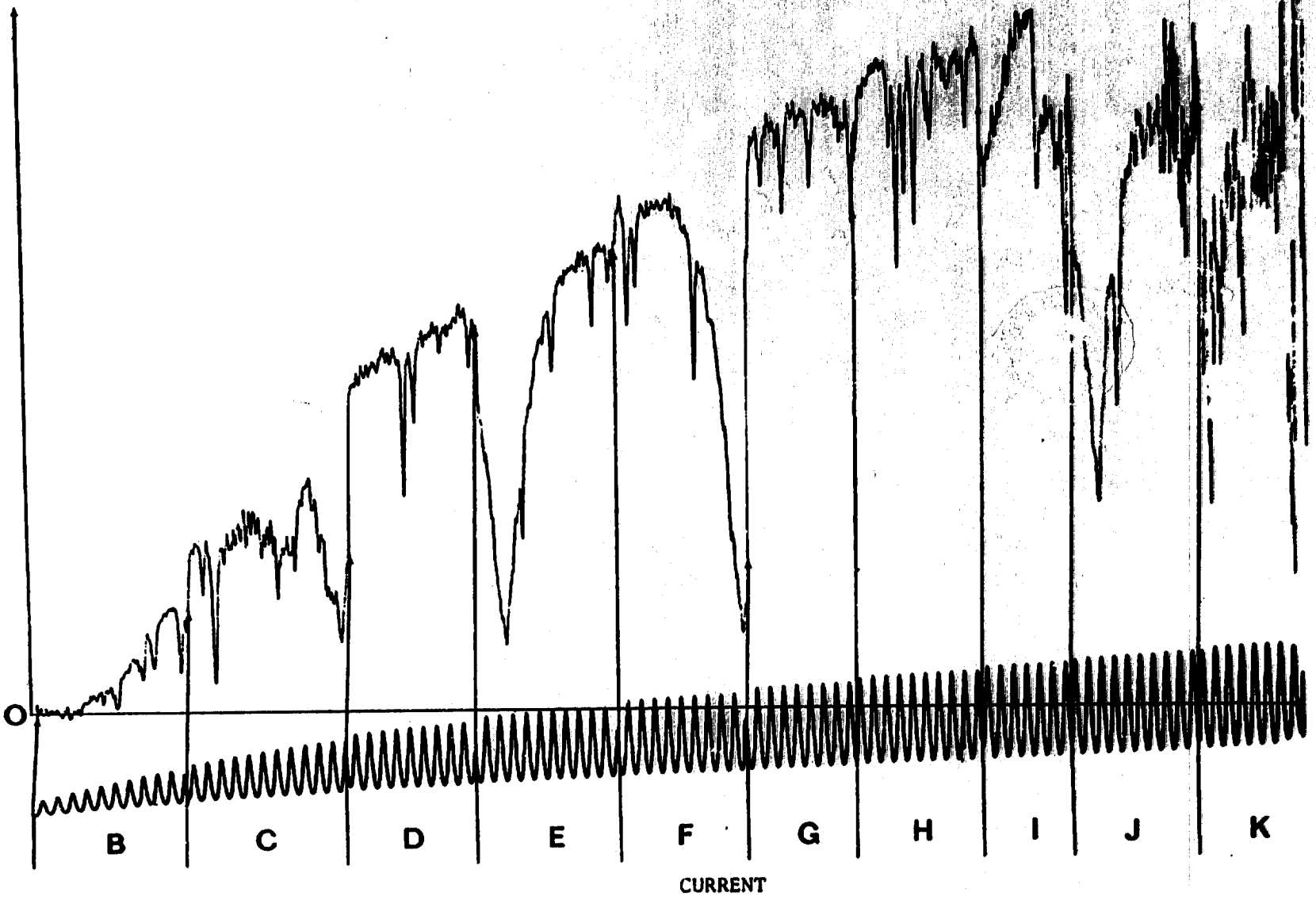

Figure 21. Heterodyne atmospheric solar absorption spectra along with etalon fringes obtained with the TDL temperature at 70.3 K. The current was scanned toward increasing currents.

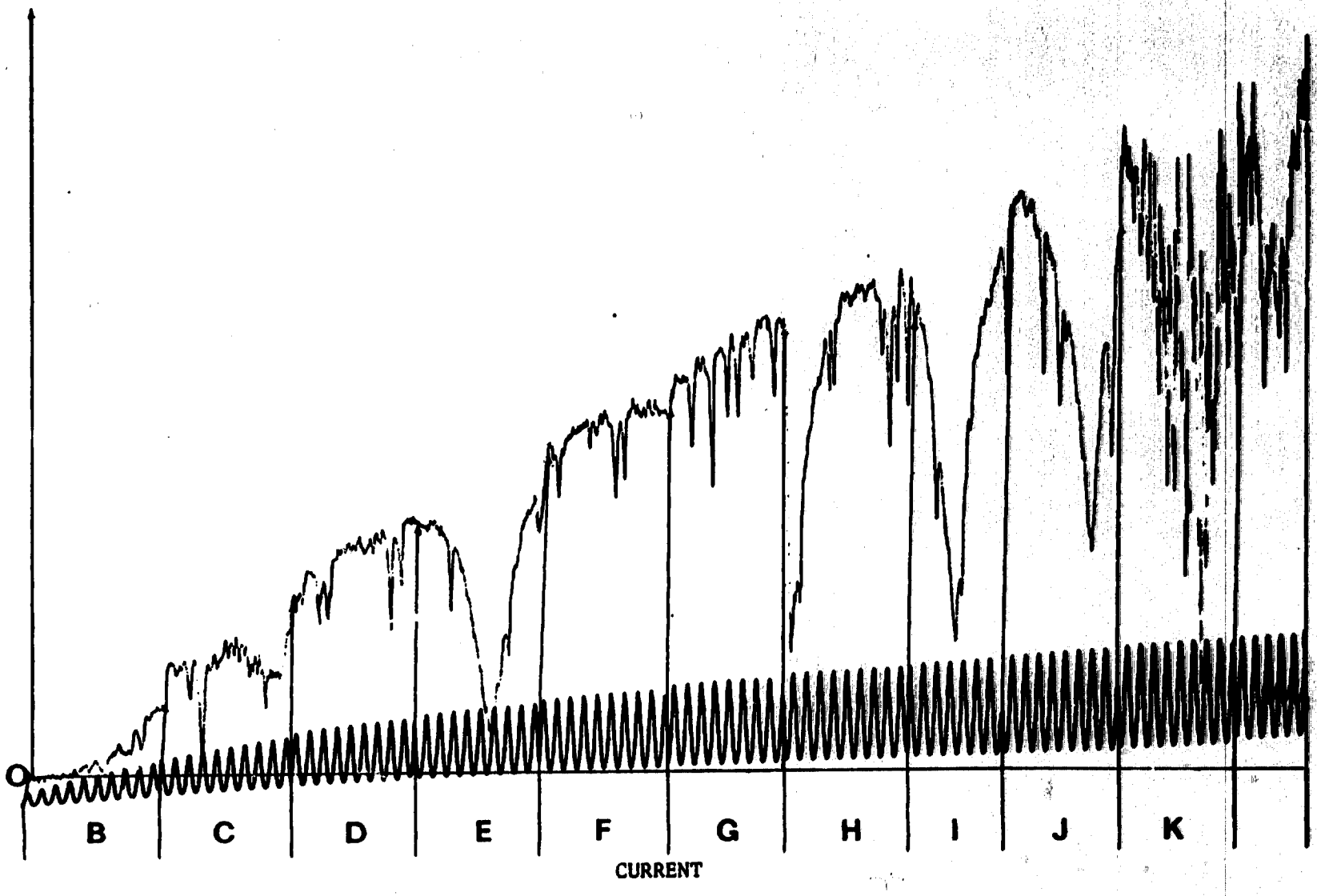

Figure 22. Heterodyne atmospheric solar absorption spectra along with etalon fringes obtained with the TDL temperature at 70.3 K. The current was scanned from high to low values.

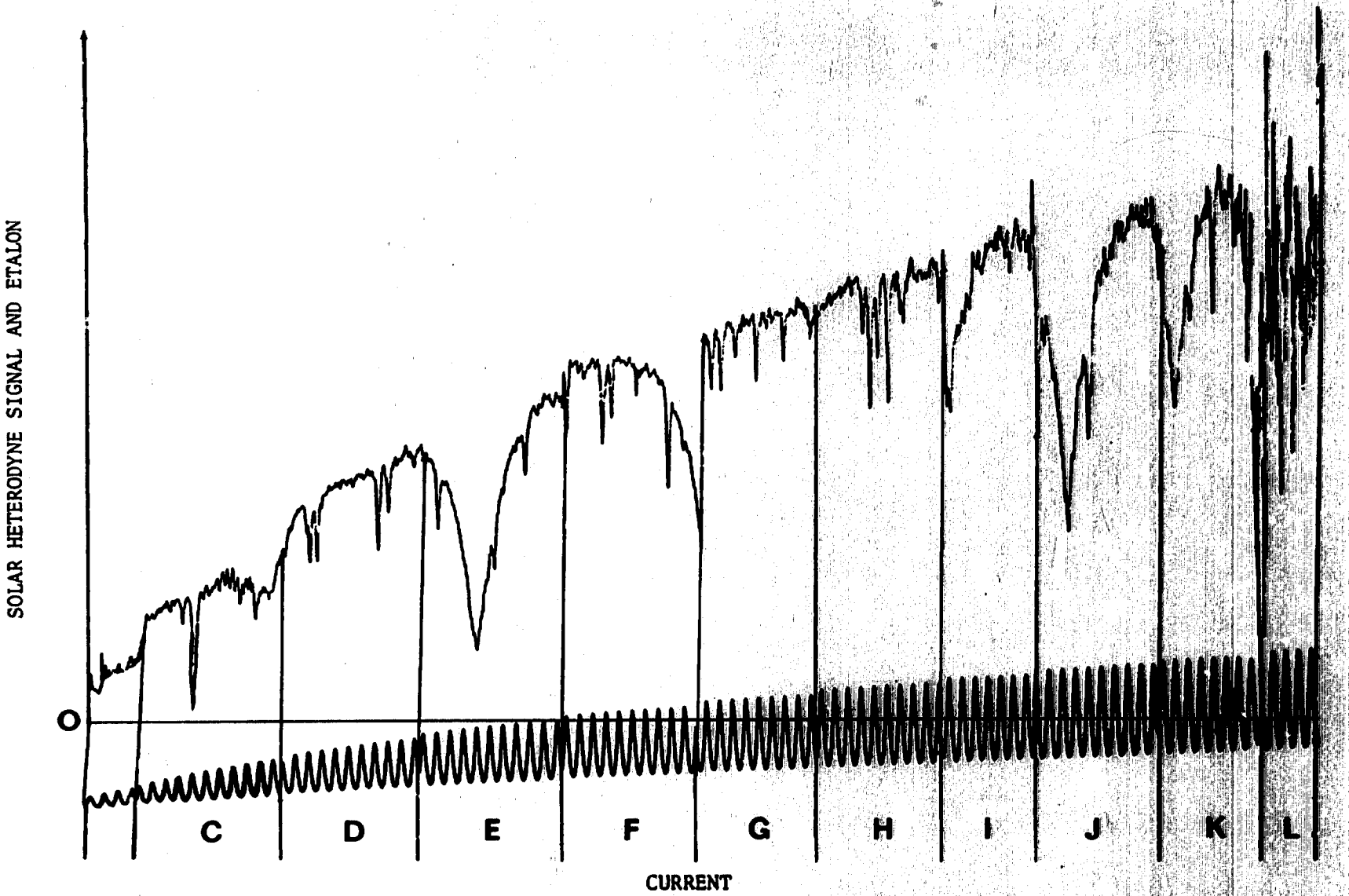

Figure 23. Heterodyne atmospheric solar absorption spectra along with etalon fringes obtained with the TDL temperature at 70.6 K. The current was scanned from low to high values.

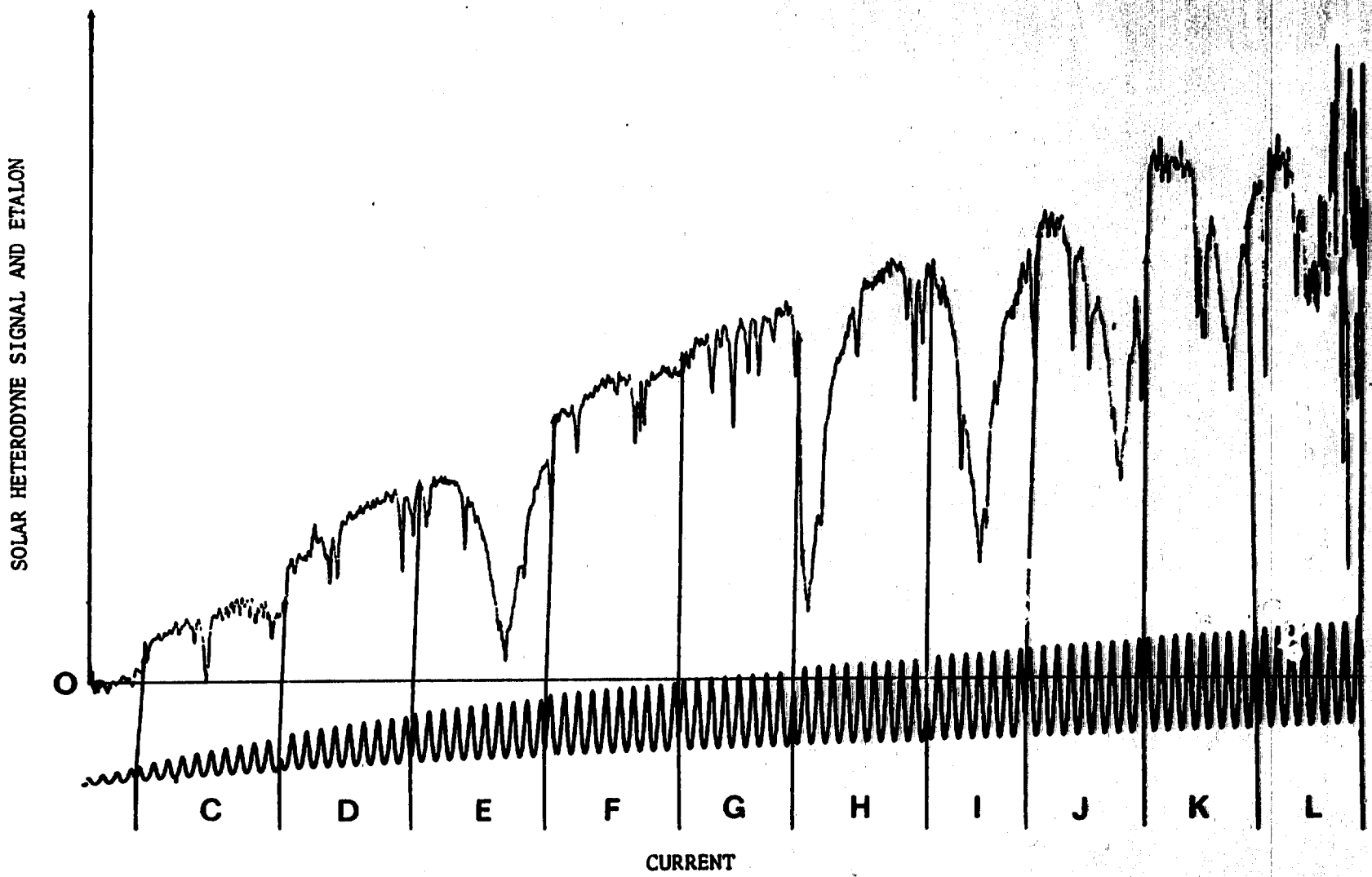

Figure 24. Heterodyne atmospheric solar absorption spectra along with etalon fringes obtained with the TDL temperature at 70.6 K. The current was scanned from high to low values.

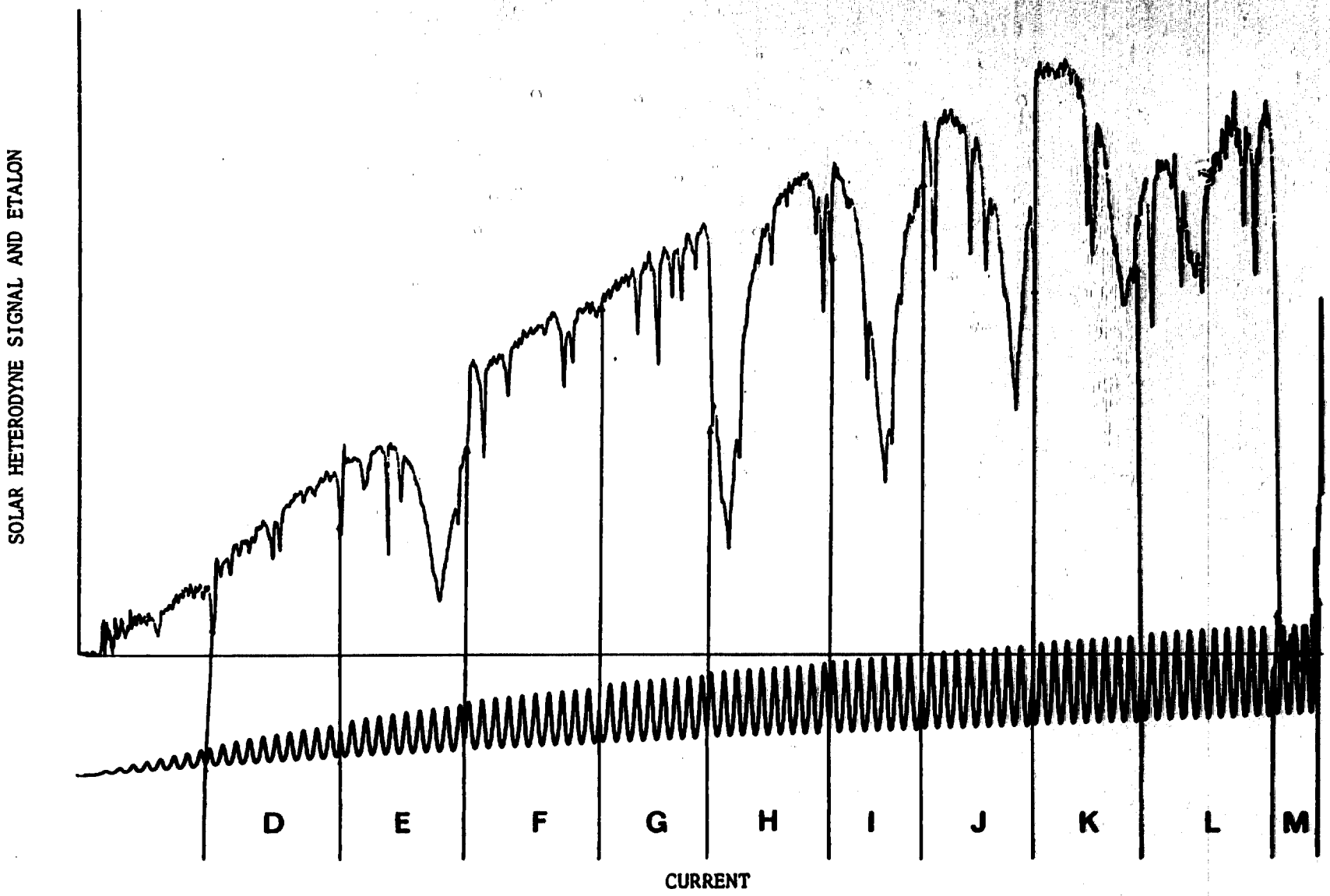

Figure 25. Heterodyne atmospheric solar absorption spectra along with etalon fringes obtained with the TDL temperature at 70.9 K. The current was scanned from low to high values.

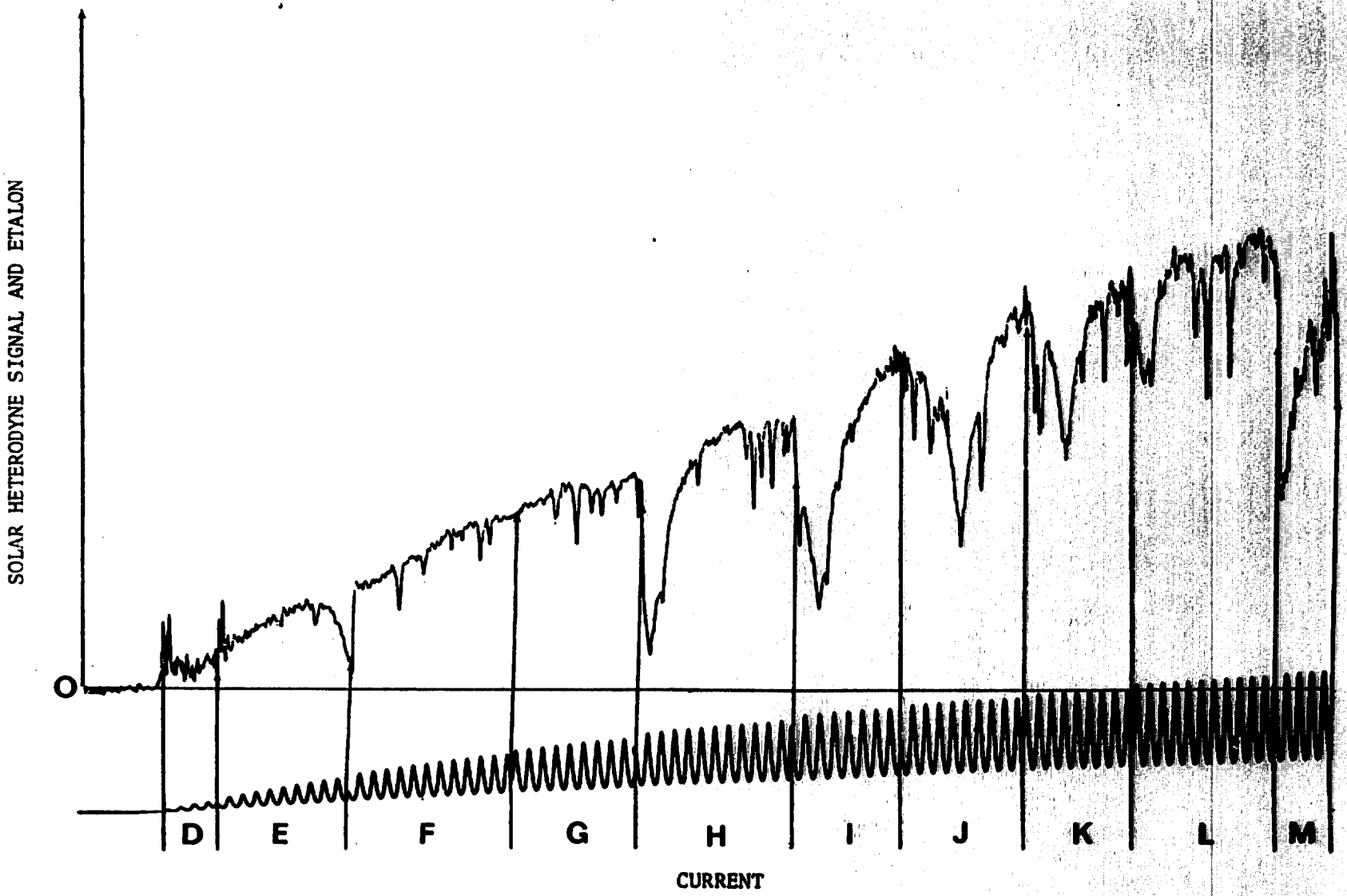

Figure 26. Heterodyne atmospheric solar absorption spectra along with etalon fringes obtained with the TDL temperature at 71.3 K. The current was scanned from low to high values.

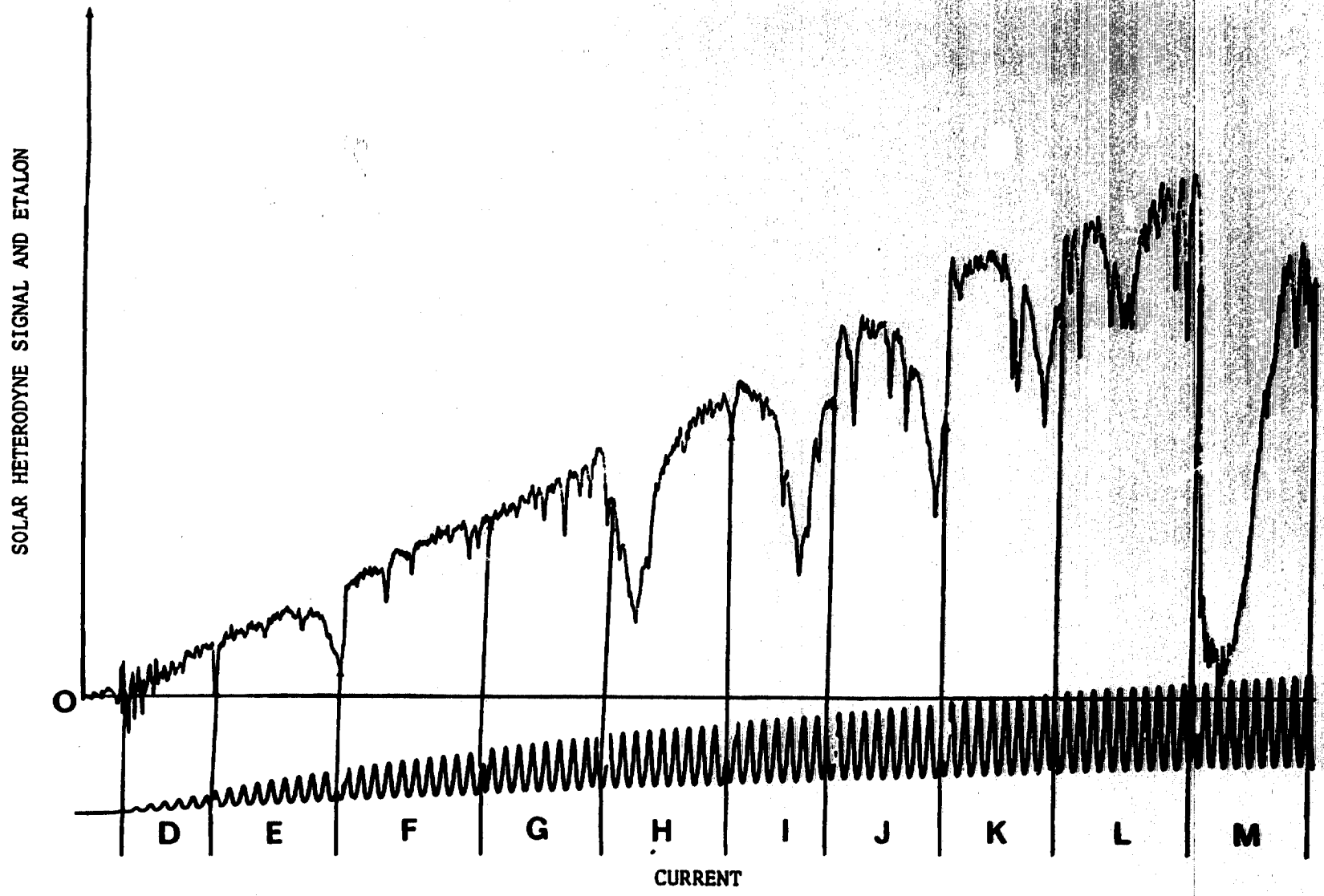

Figure 27. Heterodyne atmospheric solar absorption spectra along with etalon fringes obtained with the TDL temperature at 71.3 K. The current was scanned from high to low values.

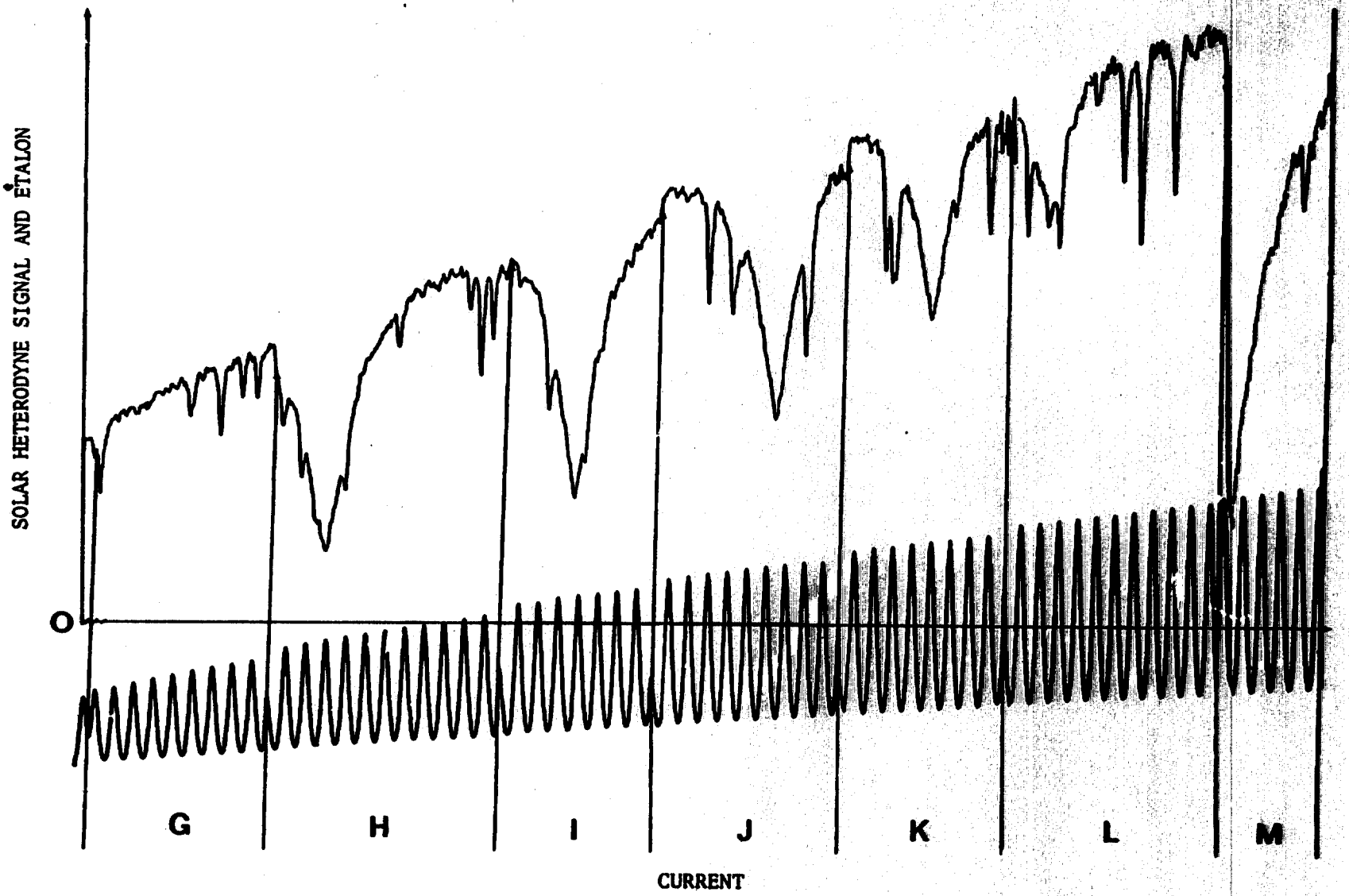

Figure 28. Heterodyne atmospheric solar absorption spectra along with etalon fringes obtained with TDL temperature at 72.0 K. The current was scanned from low to high values. Note expanded scale.

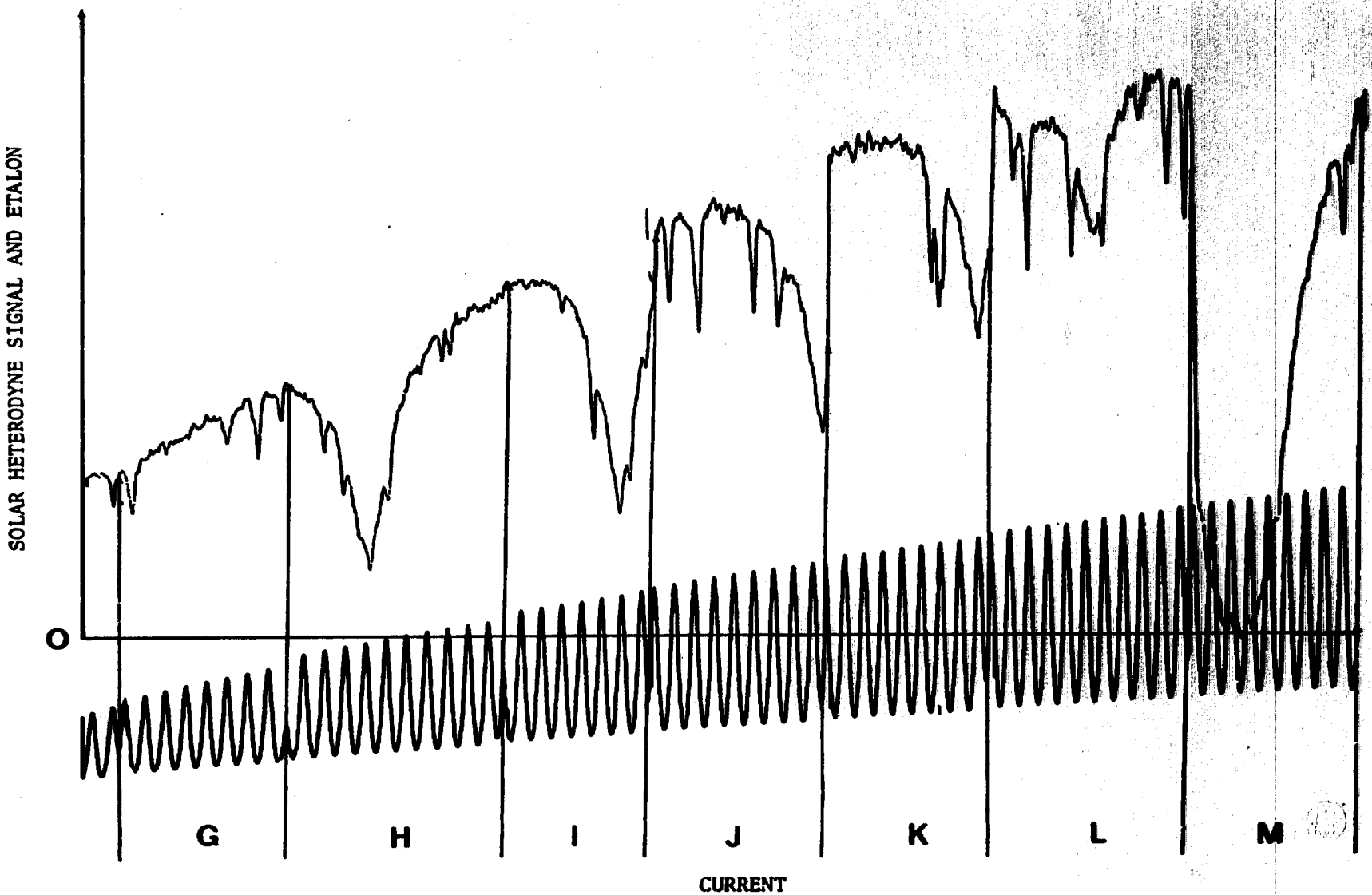

Figure 29. Heterodyne atmospheric solar absorption spectra along with etalon fringes obtained with TDL temperature at 72.0 K. The current was scanned from high to low values.

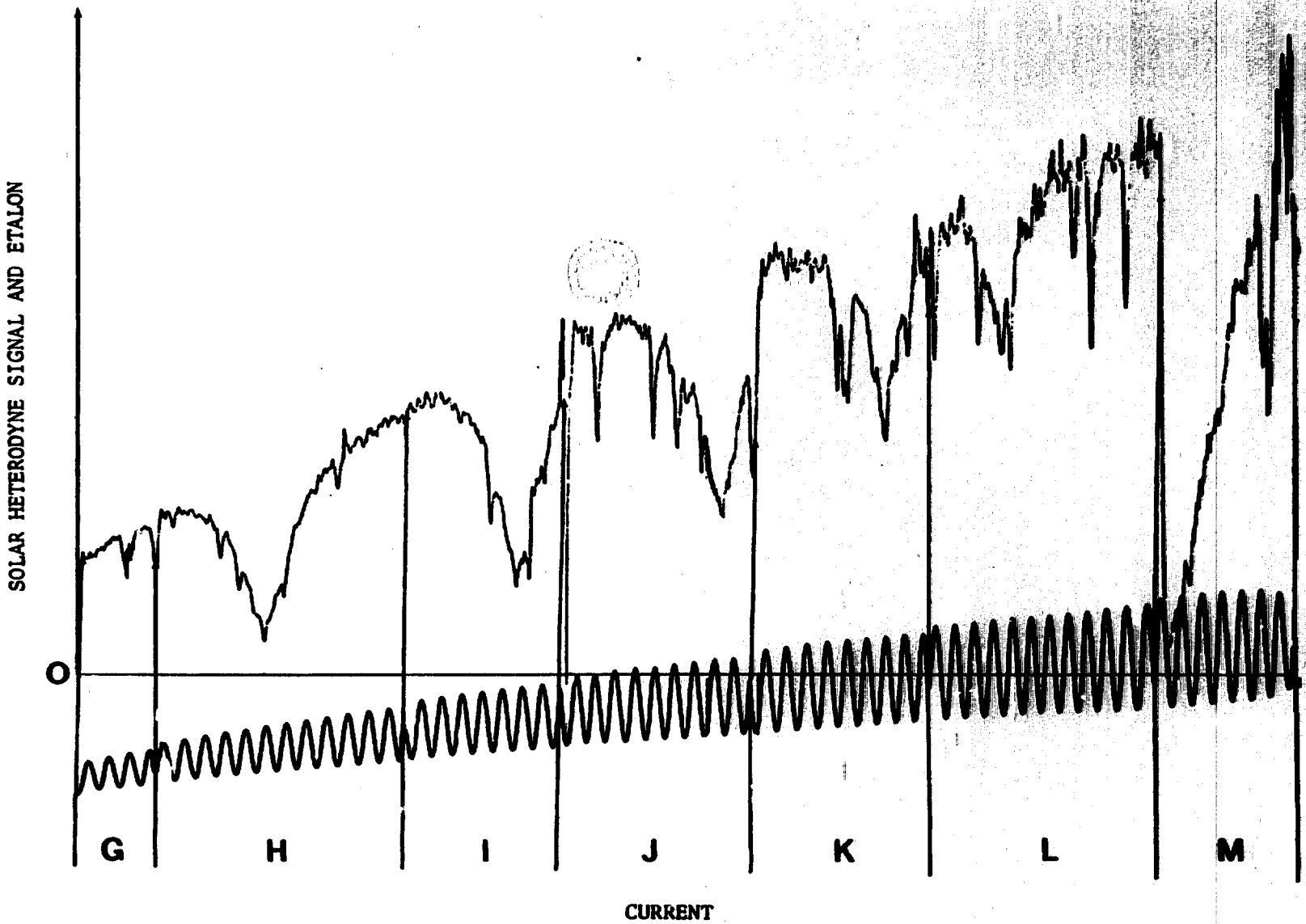

Figure 30. Heterodyne atmosperic solar absorption spectra along with etalon fringes obtained with TDL temperature at 72.5 K. The current was scanned from low to high values.

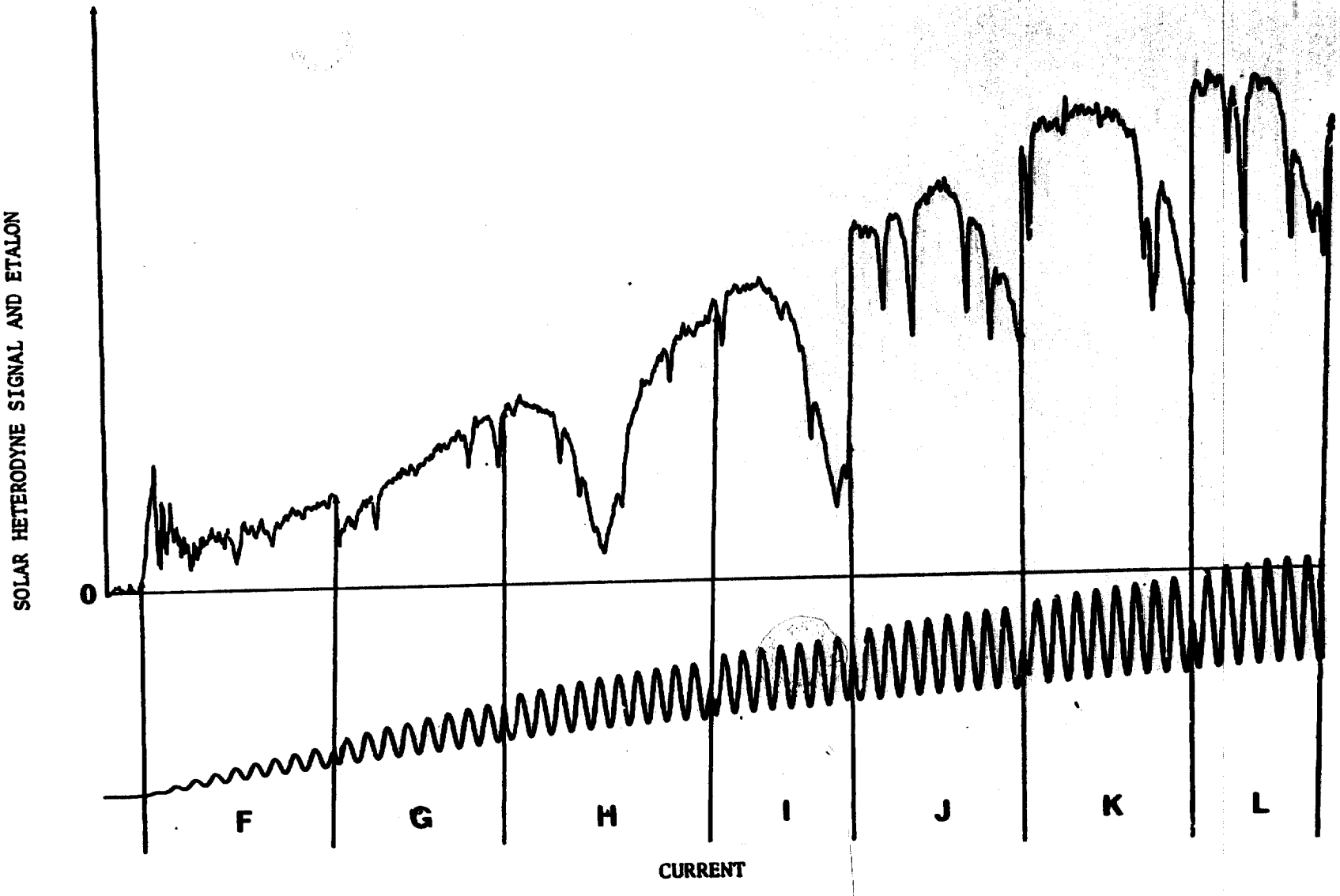

Figure 31. Heterodyne atmospheric solar absorption spectra along with etalon fringes obtained with TDL temperature at 72.5 K. The current was scanned from high to low values.

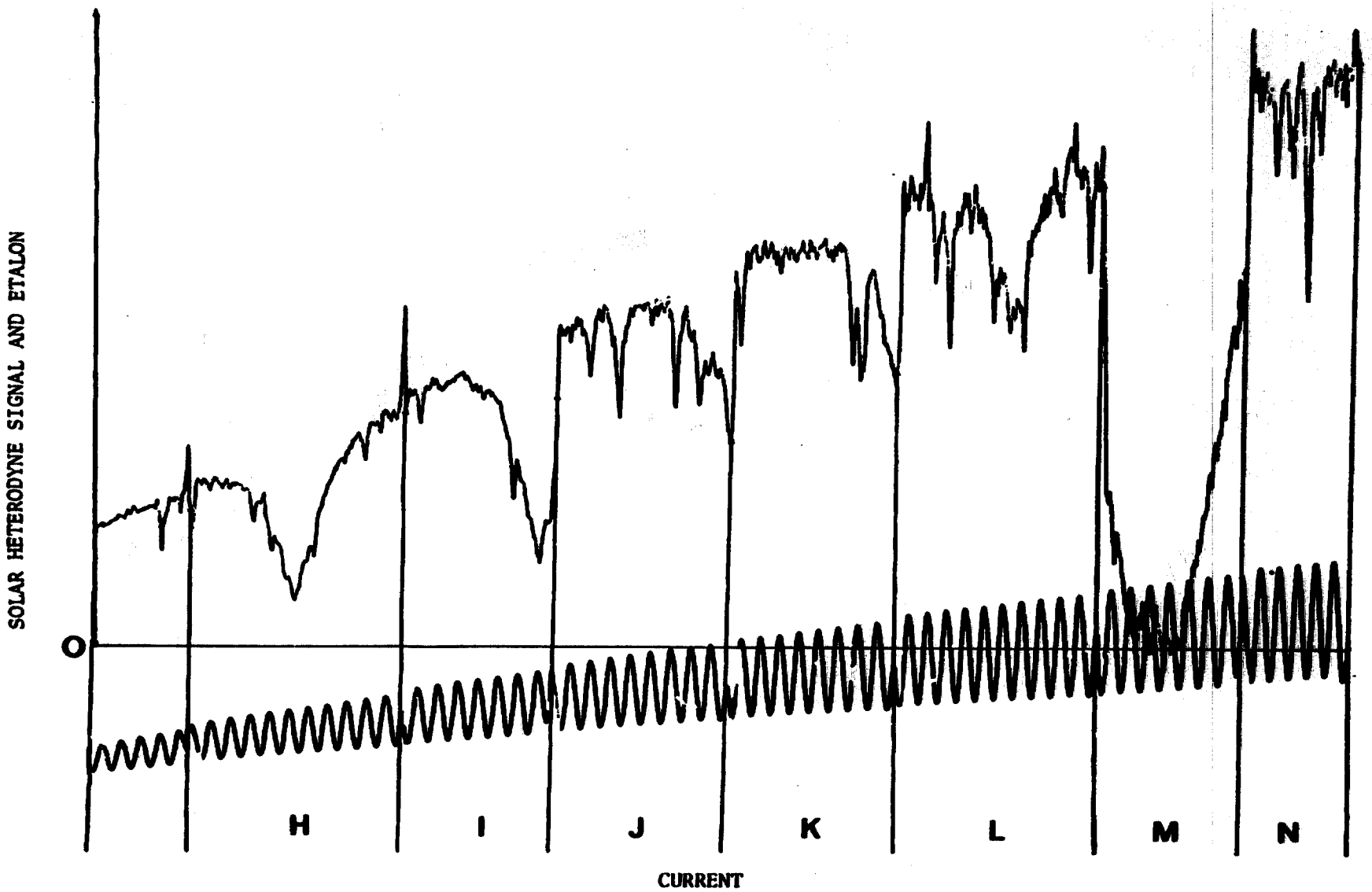

Figure 32. Heterodyne atmospheric solar absorption spectra along with etalon fringes obtained with TDL temperature at 73.0 K. The current was scanned from high to low values. Note new spectral region.

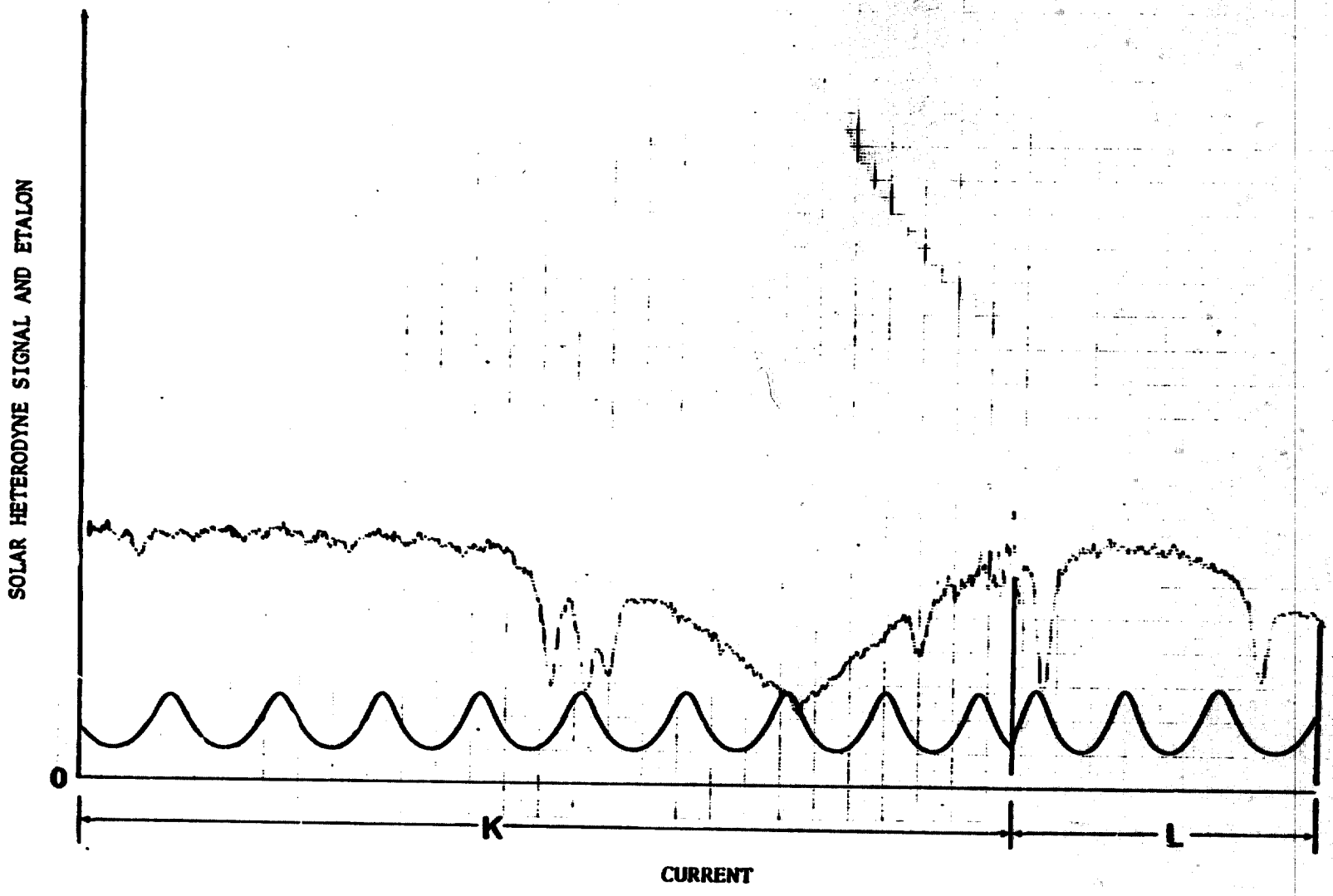

Figure 33. Expanded heterodyne atmospheric solar absorption spectra along with etalon fringes obtained with TDL temperature at 71.3 K. The current was scanned in forward direction.